2024-07-24

EVALUATING THE IMPACT OF LAND USE AND LAND COVER CHANGE ON STREAMFLOW, THE CASE OF KILTIE WATERSHED, UPPER BLUE NILE BASIN

Habtu, Kebie Melie

BAHIR DAR UNIVERSITY

BAHIR DAR INSTITUTE OF TECHNOLOGY

SCHOOL OF GRADUATE STUDIES

FACULTY OF CIVIL AND WATER RESOURCE ENGINEERING

M.Sc. THESIS

EVALUATING THE IMPACT OF LAND USE AND LAND COVER CHANGE ON STREAMFLOW, THE CASE OF KILTIE WATERSHED, UPPER BLUE NILE BASIN

By

Habtu Kebie Melie

JULY 24,2024

Bahir Dar, Ethiopia

EVALUATING THE IMPACT OF LAND USE AND LAND COVER CHANGE ON STREAMFLOW: THE CASE OF KILTIE WATERSHED, UPPER BLUE NILE BASIN, ETHIOPIA.

BY

HABTU KEBIE MELIE

A THESIS SUBMITTED TO BAHIR DAR UNIVERSITY, INSTITUTE OF TECHNOLOGY, BDU, FOR THE PARTIAL FULFILLMENT OF THE REQUIREMENTS FOR THE DEGREE OF MASTER OF SCIENCE IN HYDRAULIC ENGINEERING IN THE FACULTY OF CIVIL AND WATERS RESOURCE ENGINEERING.

Advisor:

Chalachew Abebe (Ph.D)

Bahir Dar, Ethiopia

JULY 24,2024

DECLARATION

I, the undersigned, declare that the thesis comprises my own work. In compliance with internationally accepted practice, I have acknowledged and refereed all materials used in this work. I understand that non-adherence to the principle of academic honesty and integrity, misrepresentation/fabrication of any idea/data/fact/source will constitute sufficient ground for disciplinary action by the University and can also evoke penal action from the sources which have not been properly cited or acknowledged.

Name of student: Habtu Kebie   Signature: _____

Date of submission: October 16, 2220

        Bahir Dar

This thesis has been submitted for examination with my approval as a University advisor:

Advisor

Name:Chalachew A. (Ph.D)

Signature: _____

I hereby confirm that the changes required by the examiners have been carried out and incorporated in the final thesis.

Name of Student Habtu Kebie Melie Signature _____ Date: 26 - 07 - 2024

As members of the board of examiners, we examined this thesis entitled "EVALUATING THE IMPACT OF LAND USE AND LAND COVER CHANGE ON STREAMFLOW: THE CASE OF KILTIE WATERSHED, UPPER BLUE NILE BASIN" by Habtu Kebie. We hereby certify that the thesis is accepted for fulfilling the requirements for the award of the degree of Masters of science in "HYDRAULICS ENGINEERING".

Board of Examiners

	Signature	Date
Name of Advisor		
chelachew Ayele (PhD)		26-07-2024
Name of External examiner	Signature	Date
Anwar Assefa Adem (Ph.D)		July 24, 2024
Name of Internal Examiner	Signature	Date
Demeses Alemov (Dr)		08-08-2024
Name of Chairperson	Signature	Date
Muhammed A.		26-07-2024
Name of Chair Holder	Signature	Date
Ephem Yetbarek, PhD		8-8-2024
Name of Faculty Dean	Signature	Date
Melkamu Demewez Gebeye		Aug. 8/2024
Faculty Academic Program Officer (V/Dean)		**Faculty Stamp**
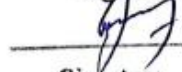
ABSTRACT

Streamflow is one of the key components of the hydrological cycle in a watershed that can be affected by a variety of variables. One of the key variables is the change in land use and land cover (LULC). This study is mainly focused on assessing the impact of LULC change on only surface runoff using the soil and water assessment tool (SWAT) model. Sensitivity, calibration, and validation were performed by SWAT-CUP (calibration and uncertainty program) using sequential uncertainty fitting version 2 (SUFI-2). The time series LULC map of the research area for the years 1997, 2010, and 2022 were assessed using Google Earth Engine (GEE). There were four different algorithms applied to classify the LULC change (SVM, CART, RF, and Navia's) available in GEE and the coverage of LULCs was including land class of agricultural land, forest land, grass land, urban area, barre land, and shrub land. The best performing of four distinct algorithms were compared, and chosen to generate LULC map. To train and evaluate the LULC map generated from the GEE platform, high-resolution, 30 meter Landsat imagery from Landsat 5 Thematic Mapper (TM), Landsat 7 Enhanced Thematic Mapper (ETM), and Sentinel 2 were employed, along with historical trends and ground-based data. As a result, the RF algorithms performed well. During the study period, the area covered by agriculture increased from 48.09% to 64.51%, while forest cover increased from 1.52% to 5.51% and grass land declined from 32.31% to 8.81%. The calibration and validation result showed that an acceptable range between observed and simulated streamflow (0.83 for NSE and 0.83 for R^2) and (0.77 for NSE and 0.80 for R^2) respectively. LULC changes have an impact on the streamflow of the Kiltie watershed by changing surface water quantity increased by 20,971,440 m^3 at wet and decreased by 3,090,528 m^3 at dry season.

Key words: SWAT, SWAT-CUP, Streamflow, Google Earth Engine, Machine Learning, Kiltie Watershed

TABLE OF CONTENTS

LIST OF ABBREVIATION

API	Application Interface Program
CN	Curve number
DEM	Digital elevation model
DMC	Double mass curve
ETM	Enhanced thematic map
FAO	Food and agricultural organization
GEE	Google Earth Engine
GIS	Geographical Information System
GPS	Geographical positioning system
HRU	Hydraulic response unit
LULC	Land use land cove
NMSAE	National metrological service agency of Ethiopia
NSE	Nash Sutcliffe simulation efficiency
RF	Random forest
RS	Remote sensing
SCS	Soil conservation service
SVM	Support vector machine
SWAT	Soil and water assessment tool
SWAT- CUP	Soil and water assessment tool calibration and uncertainty programs
TM	Thematic map
USGS	United States Geological Survey

LIST OF FIGURE

LIST OF TABLE

1   INTRODUCTION

1.1   Background

Throughout human history, land use has been tightly attached to economic, social, infrastructure, and other human activities (Lambin et al., 2003). In the past few decades, the conversion of grassland, woodland, and forest into agricultural land and pasture lands has risen dramatically, especially in developing countries where a large proportion of the population depends on natural resources for their livelihoods (Siry et al., 2005). The current rate of change is not the same as what it was at the beginning.

Understanding the hydrological process associated with land use and land cover (LULC) change is vital for decision-makers to improve human wellbeing. LULC change is one of the factors that directly impact the watershed hydrological cycle (Brook et al., 2015), and the change significantly affects the hydrology of the landscape, caused by anthropogenic activities (Engida et al., 2021). LULC changes are mainly caused by unlimited human interest activities as a result of an increase in human population without considering its consequences on surface water balance. One of the main parameters that affects the surface water quantity and groundwater table in a watershed is the use of land, and its cover changes over time. The response of hydrologic circulation is closely related to land use planning and management (Garg et al., 2019). On top of the rapid change in LULC of forest land, grazing land or bush lands to cultivated lands is becoming a common practice in most parts of Ethiopia (Abate & Lemenih, 2014). The impacts of LULC change on hydrology are especially significant, as they are related to the change and availability of water resources that are essential for both human beings and ecosystems (Oki & Kanae, 2006). The progressive vegetation removal and increased impervious area in the watershed resulted in increased wet-season runoff frequency and magnitude.

Hydrological data collected throughout the year is important for understanding and measuring the impact of land use and land cover changes on the watershed. In Ethiopia, there is a lack of metrological and hydrological data, especially for small watersheds. Because of this, hydrology studies are difficult because of some input data. This leads to the prediction of data for research and design work from the nearest watershed using hydrological models.

Reliable continuous streamflow forecasting using hydrological modeling is an important factor in watershed planning and sustainable water resource management because it is instrumental in obtaining a deeper sense of the flow variability of the watershed. However, it becomes challenging as the majority of rivers and streams in the world are ungauged or poorly gauged (Razavi & Coulibaly, 2013). Ungauged streams are often located upstream (in mountainous areas and maritime regions) and downstream in rural and remote areas because of their inaccessibility or lack of developer intentions. However, the hydrological parameters for the catchment can be predicted using regionalization methods (Sivapalan et al., 2003). This study was conducted in one of the short-period gauged rural areas of the Kiltie watershed, Gilgel Abay River Basin, in North Gojjam Zone of Amhara Region.

Various models have been developed and applied to predict, assess, and monitor natural phenomena such as streamflow from the watershed, but the SWAT model, which is a deterministic, continuous watershed model that can operate on monthly and daily time steps, is the most widely used and freely available (Neitsch, 2005). The SWAT model is the best of the hydrological models because of its availability to apply to large-scale watersheds (> 100 km^2), interface with a Geographic Information System (GIS), continuous-time simulation performance, generation of the largest number of sub-basins, and ability to characterize the watershed in sufficient special detail. In this study, the SWAT model is used to analyze the impact of LULC on surface runoff.

1.2 Statement of the problem

Tana sub-basin has been continuously under threat by several land resource degradation which is caused invariably by a combination of natural phenomenon and man's action such as destruction of the forest resources through deforestation, overgrazing and inappropriate agricultural practices that are not in harmony with the ecological environment (Andualem & Gebremariam, 2015). The main factor that contributes to land degradation is continuous and active land use and land cover change, especially from vegetation to other land use types, typically cultivated land. This continuous change in land cover has impacted the water balance of the watershed by changing the magnitude

and pattern of the component of streamflow which results increasing the extent of the water management problem (Geremew, A. A. 2013). Deforestation is a day-to-day activity of people living in rural watersheds, and it causes the majority of environmental degradation by increasing surface runoff instead of infiltration into the soil. Therefore, these events resulted in a decrease in river base flow in the watershed. This study considered the LULC change periods between 1997 and 2022 of the Kiltie watershed which is one of the tributary of Gilgel Abay watershed. Hence, a strong need is identified for the hydrological techniques and tools that can assess the effect of LULC change on surface runoff of a watershed. Such techniques and tools can provide information that can be used for water resource management at a watershed. This study is designed to investigate the impact of LULC change on streamflow of the Kiltie watershed, Sub-Tana Basin by using SWAT model.

1.3 Objective

The study aims to assess the impact of land use and land cover changes on the surface runoff of the Kiltie watershed using the Soil and Water Assessment Tools (SWAT) model.

The specific objective includes:

> ➢ To evaluate the machine learning algorithms for LULC classification.
> ➢ To identify the main LULC classes and their changes.
> ➢ To evaluate the effect of land use and land cover changes on the streamflow of the Kiltie watershed for the past years by using the SWAT model.

1.4 Research questions

To address the above objectives, the following research questions are designed:

1. Which machine learning classifier is appropriate for the classification of LULC for Kiltie Watershed?
2. What are the main LULC types, their area coverage in the Kiltie watershed?
3. How do land use and land cover change affect the annual flow of the Kiltie River?

1.5 Scope of the study

This study was limited to the Kiltie watershed and focuses only on the assessment of land use and land cover change and its impact on the streamflow of the watershed. The study

area is one of the tributary watersheds, the Gilgel Abay watershed, and the river joins the Gilgel Abay River after the Wottet Abay gauging station. The SWAT model is used to analyze the impact of LULC changes on streamflow. The LULC change and map were identified using the Google Earth Engine (GEE) application for the periods of 1997, 2010, and 2022. This study only focuses on the impact of LULC change on streamflow.

1.6   Significance of the study

Giving less attention to LULC change assessment leads to poor planning, design, and operation of water resource projects and soil conservation works at the watershed level. Such an outcome affects directly or indirectly the economic development of the country. So, a proper estimate of LULC change and the identification of different analyses of the area increase knowledge about river base flow within the watershed. Therefore, this study contributes to assessing the impact of LULC change on surface runoff in the Kiltie watershed for future water resource developments and soil conservation works and also clarifies the LULC impacts on streamflow in the watershed. The main significance of this study is to understand the impact of LULC change on water resource. The findings of this study will give scientific clues for resource-based analysis and the development of effective and appropriate response strategies for sustainable management of natural resources.

2 LITERATURE REVIEW

2.1 LULC definition and concept

Land use is the utilization of land by human activities for agriculture, settlement, and other purposes as they want. Vandewiele & Elias, (1995) defined land use as a human endeavor to alert the future of land to create a favorable environment for their lives by engaging in various activities such as agricultural land, road construction, and settlement. According to the author, environmental issues are tied to land use change. Therefore, LULC change analysis is required for environmental management through decision-making and future planning.

Global scale studies have been conducted on LULC change and its impact on streamflow. For example, Shahid et al. (2018) conducted a study on the impacts of climate change and human activities on stream flow using the ABCD hydrological model. The model was employed to examine how land use and climate change affected runoff generation at the basin level in   Pakistan. Previous studies in the Awash basin and elsewhere in Ethiopia identified the impact of LULC change on surface runoff (Woldesenbet et al. 2017; Gashaw et al. 2018; Birhanu et al. 2019; Dibaba et al 2020). These studies focused on analyzing the impact of climate change and land use change on runoff and runoff changes using diverse methodologies. Studies also tried to assess the impact of LULC change on surface water availability (Kumar et al. 2018; Tadese et al. 2020b). These studies contributed to the current understanding of the impact of LULC changes on surface runoff and the water availability in the watershed. However, they are presented in a disentangled way, and the exact relationship between the impacts of LULC change on streamflow and hence the surface water availability is missing.

Land cover refers to the visible physical characteristics of the earth surface, such as water bodies and vegetation, as well as those created by human activities, such as settlement areas, agricultural land, urbanized land features, exposed land surfaces due to tree removal for plantations, and others (Potopová et al., 2017). Land use and land cover

changes result from various natural and human factors within social, economic, and political contexts. Hence, the local human activities expressing the drivers can be determined by measuring the rates and types of changes and analyzing other relevant sources of data like demographic profiles, household characteristics, and policies related to land resource administration (Di Gregorio, 2005).

According to Takassahun et al. (2009) LULC change is commonly grouped into two broad categories: conversion and modification. Conversion is defined as a change from one cover or use category to another (for example, from forest to grassland). Modification, on the other hand, represents a change within one land use or land cover category (for example, from a rain-fed cultivated area to an irrigated cultivated area) due to changes in its physical or functional attributes. These changes in LULC systems have important environmental consequences through their impacts on soil and water, biodiversity, and microclimate (Meyer & BL Turner, 1994).

Considering the research on land use change alone, the development of separate and very sophisticated land dynamic tools were caused by the large number of variables from different scientific fields that influence land use change. Therefore, future development of land use change modeling related to river catchment modeling will probably remain a parallel process where a dynamic link would be the desired connection from a long-term perspective dealing with dynamically changing land use input.

2.1.1 Causes of LULC change

LULC changes are complex processes that arise from variations in the land cover during the land change process. According to Lumbin et al. (2003), LULC change is driven by the interaction in space and time between biophysical and human dimensions. Throughout the entire history of mankind, intense human utilization of land resources has resulted in significant changes in LULC. Since the period of industrialization and rapid population growth, LULC change phenomena have strongly accelerated in many areas. There is a significant statistical correlation between population growth and LULC conversion in most African, Asian, and Latin American countries (Gereta et al., 2003). In most developing countries like Ethiopia, population growth has been a dominant cause of LULC change compared to other forces (Meyer & BL Turner, 1994). Due to the

increasing demands of food production, agricultural lands are expanding at the cost of natural vegetation and grasslands (Pretty et al., 2010). The expansion and increase of agricultural lands, the development of urban areas, and the need to extract timber and other products are accelerating over time to meet the needs of an increasing population.

2.1.2 Criteria for land use and land cover classification

A land use and land cover classification system that can effectively employ orbital and high-altitude remote sensor data should meet the following criteria:

- ➢ The minimum level of interpretation accuracy in the identification of land use and land cover categories from remote sensor data should be at least 85 percent.
- ➢ The accuracy of interpretation for the several categories should be about equal.
- ➢ Reputable or repetitive results should be obtainable from one interpreter to another and from one time of sensing to another.
- ➢ The classification system should be applicable to extensive areas.
- ➢ The classification system should be suitable for use with remote sensor data obtained at different times of the year.
- ➢ The categorization should permit vegetation and other types of land cover.
- ➢ Effective use of subcategories that can be obtained from ground surveys or from the use of larger-scale or enhanced remote sensor data should be possible.
- ➢ Aggregation of categories must be possible.
- ➢ Comparison with future land use data should be possible.
- ➢ Multiple uses of land should be recognized when possible.

2.1.3 LULC change detection

LULC change detection can be defined as the process of identifying differences in two or more images of the same location taken at different times. Principally, it also involves the ability to quantify temporal applications of remotely sensed data obtained from Earth-orbiting satellites (Lambin et al., 2003). Many change detection methods were developed and used for various applications. However, the change detection techniques can be broadly divided into two approaches: pre-classification and post-classification.

In the pre-classification approach, the image values are not categorized for the change analysis. The most common and widely used pre-classification approach is vegetation

index difference (NDVI), normalized difference water index (NDWI), change vector analysis (CVA), etc. They are simple, effective at detecting and locating change, and simple to execute. Post-classification approaches separate images and assess the differences of images pixel by pixel, providing comprehensive change-class information that is critical for landscape monitoring.

In general, selecting an appropriate approach to detecting change is critical because no single method can be used effectively for all research topics. The result of change detection from imagery can be affected by several factors, such as the quality of image registration between multi-temporal images (Tingting Dan, 2018), change detection methods, and lack of knowledge about approaches as well as analysis skill and experience (Shivangi Mishra, 2017), dataset availability and quality (Ayele, 2016), image pre-pprocessing (Khorram, 2013), the atmospheric conditions and shadow present in the image (Gustavtolt, 2011), the acquisition times of the image (Khorram, 2013), and landscape and topography characteristics of the study areas.

2.1.4 Impact of LULC change on streamflow

Watershed characteristics directly affect the river flow. The flow of the stream and the amount of water moving off the watershed into the stream channel have a direct relationship. Watersheds that have a large coverage area have the potential to generate large river flows because they have a large capacity to store water. LULC plays a key role in monitoring the hydrologic response of watersheds in several important ways. Changes in LULC can lead to significant changes in evapotranspiration, soil moisture content and infiltration capacity, surface and subsurface flow regimes, including base flow contributions to streams, groundwater recharge, surface roughness, runoff, and soil erosion through complex interactions among vegetation, soils, geology, topography, and climate processes.

Therefore, LULC can affect both the degree of infiltration and surface runoff following rainfall events and rates of evaporation. Surface water flow and ground water flow can be affected by LULC changes. This evidence indicates that LULC is important to determine the potential of water supply in its transit through a landscape.

(Zaitunah & Manurung, 2018), suggested that decreased evapotranspiration due to deforestation is larger than the increase in evapotranspiration due to irrigation when globally averaged. (Tingting Dan, 2018), emphasized that the observed increase in runoff over the 20th century was not only due to climate change but that LULC change was equally important. Both surface runoff and groundwater flow are significantly affected by types of LULC (Gordon et al., 2005).

Several studies have been conducted to investigate the impact of LULC changes on streamflows, which ended up exhibiting that the causes of streamflow changes are due to LULC changes. A study on LULC changes impacting streamflow by Piao et al. (2007) in the Upper Mara watershed showed that the conversion of forest to agriculture decreased the dry season flow, which resulted in aggravating water scarcity during low flows.

All parts of the literature have shown that there is a strong relationship between streamflow and LULC change. Assessing the impact of LULC changes on the hydrology of the Gilgel-Abay watershed in the Lake Tana basin also came up with similar findings (Geremew, A. A. 2013). In the wet season, streamflow in Gilgel Abay has increased by 16.26 m3/sec and decreased by 5.41 m3/sec in the dry season.

2.2 Land use and land cover change in Ethiopia

Several studies have been conducted in different locations in Ethiopia using various approaches and methods for studying LULC changes. For instance, Asitatikie, (2019), investigated how LULC change affects the hydrology of the Rib catchment in the Lack Tana sub-basin. The study discovered a 29.94% increase in cultivated land and a 6.143 m3/s increase in streamflow.

Fentie et al., (2020), do another investigation to investigate LULC variations and their cumulative effects on the chemical and physical qualities of soils within the Tejibara watershed over 30 years (from 1989 to 2019). In the investigation, the amount of forest and grazing land has decreased, creating changes in soil attributes. As a result, the land has been degraded, and soil productivity has decreased.

(Dinka & Chaka, 2019), conduct a similar study on the Adei watershed in Ethiopia's central highlands. Significant LULC change has occurred in the watershed, particularly the conversion of natural cover to managed agrosystems. Furthermore, the report stated

that farmland has rapidly expanded, resulting in plant diversity and the emergence of deforestation as a result of this expansion.

Overall, global LULC change is accelerating, particularly in developing countries like Ethiopia. It has a wide range of consequences, from climate change to biodiversity loss. As a result, it's critical to assess the shifting trend and its implications in Ethiopia as a whole, as well as in the Kiltie watershed in particular.

2.3   Analysis of Land Use Land Cover Change

2.3.1   Image classification

Image classification is perhaps the most important part of digital image analysis. It is very nice to have a "pretty picture" or an image showing a magnitude of colors illustrating various features of the underling terrain, but it is quite useless to know what the colors mean. Image classification is used to identify and portray, as a unique gray level or color, the features occurring in an image in terms of the object or type of land cover these features actually represent on the ground. The intent of the image classification process is to categorize all pixels in a digital image into one of several land cover classes. This categorized data may then be used to produce thematic maps of the land cover present in an image. Normally, multispectral data is used to perform the classification, and indeed, the spectral pattern present within the data for each pixel is used as the numerical basis for categorization.

Information derived from land use and land cover change detection is important to land conservation, sustainable development, and the management of water resources (Dires 2019). To perform image classifications, the raw data must be preprocessed and prepared properly so that errors due to the geometry of the earth and radiometric and atmospheric effects can be accounted for. The general procedure in the preprocessing stage includes the detection and restoration of band lines, geometric rectification or image registration, radiometric calibration, atmospheric correction, and topographic correction. With the availability of historical remote sensing data, reduced cost, and increased resolution from satellite platforms, remote sensing technology appears ready to make a greater impact on monitoring LULC. LULC can be analyzed over a period using Landsat sensors such as Landsat Multi-Spectral Scanner (MSS) data and Landsat Thematic Mapper (TM) data

using image classification techniques (Webister, 2010). Since 1972, Landsat satellites have provided repetitive, synoptic, and global coverage of medium-resolution multispectral images. Image classification using remote sensing has attracted the attention of the research community (Lu D. A., 2007).

There are two main classification methods: unsupervised classification and supervised classification.

A. Supervised classification

During supervised classification, the classifier or expert identifies examples of the information classes, i.e., land use type, of interest in the image, which are called training sites. Then the image processing software system is used to develop a statistical characterization of the reflectance for each information class. This stage is often called signature analysis and may involve developing a characterization as simple as the mean or the average of reflectance on each band.

The objective is to extend or extrapolate information on land cover type for a known area of the image to the unknown areas of the whole selected image. The image analyst defines a number of training areas for each land cover category. Based on this information, the computer generates spectral signatures.

In supervised image classification, the analyst has previous knowledge about pixels to generate representative (ground truth) parameters for each land cover class of interest. The maximum likelihood classification, under the category of supervised classification, is the most widely used per-pixel method by taking into account the spectral information of LULC classes (Qian, 2007).

B. Unsupervised classification

Unsupervised classification is a method that examines a large number of unknown pixels and divides them into a number of classes based on the natural groupings present in the image values. Unlike supervised classification, unsupervised classification does not require analyst-specified training data. The basic premise is that values within a given cover type should be close together in the measurement space, i.e., have similar gray levels, whereas data in different classes should be comparatively well separated Lillesand and Kiefer (1994).

Unsupervised classification is the simplest technique within the image data. For the different wavelengths, the computer is asked to determine a user-defined number of clusters. Each cluster represents a land cover class or sub-class. The mean digital value for each input band could be represented as a spectral reflectance profile. The cluster represents the spread of values around the mean for the land cover class. After the classification has been completed, each class should be examined and assigned a name. It may also be necessary to merge a number of classes into a single category.

Unsupervised classification is an automated classification method that creates a thematic raster layer from remotely sensed data by letting the software identify statistical patterns in the data without using any ground truth data (Lilleesand 2004).

2.3.2 Application of Google Earth Engine for LULC Change Detection

Google Earth Engine (GEE) is a geographical processing tool with a cloud-based platform for wide-ranging environmental study and interpretation. The GEE is a web-based Graphical User Interface (GUI) that provides access to a multi-petabyte catalog of RS imagery and other datasets through Google computational infrastructure. For popular coding languages like JavaScript and Python, a set of application programming interfaces (APIs) and development environments are available. GEE is a powerful cloud computing platform that provides the whole Landsat collection and allows for rapid scientific analysis and expert analysis (Navarro, 2017). It allows scientific researchers and developers to visualize a large geographical dataset using advanced machine learning algorithms. Massive satellite images can be directly obtained from this platform, and image processing can be evaluated and executed using machine learning algorithms (Tsai, 2018).

GEE Explorer and Code Editor are two web-based platforms that are currently available to anyone who has registered to use them (Gorelick, 2017). GEE has been used in a variety of studies because it is a new application. GEE contains a wealth of data from satellites, ranging from the Landsat program to a variety of climate datasets.

GEE has been used in a variety of applications. These will be used to analyze LULC change and provide a suitable foundation for additional investigation on a separate platform (Wahap, 2020). The application of GEE is very wide, ranging from drought

assessment (Sazib, 2018), agriculture and ecosystem service (Goldblatt, 2017), drought monitoring, vegetation mapping, and monitoring (Poortinga, 2018), to historical LULC mapping (Geetha, 2019)

Generally, all studies agree that GEE is capable of creating multi-temporal maps or conducting time series analysis using the available satellite images on the platform. The GEE platform could be very useful and rapid for analyzing satellite images and doing remote sensing analysis of large and long-term data. The GEE has many advantages. The major benefit is that the data is preprocessed and ready to use, and a large number of processed and unprocessed data can be maintained effortlessly (Gorelick, 2017). Because the GEE's easily accessible and user-friendly properties provide a convenient environment for interactive data and algorithm development, users may contribute and construct their data and collections using Google's cloud resources to execute all of the processing (Mutanga, 2019).

The main limitation of the GEE platform is its dependency on an internet connection and filtering the cloud. In the wet season, it is very difficult to get an image that is free from cloud cover using the cloud cover masking function available on GEE.

2.3.3   Machine learning classification in GEE

Machine learning algorithms organize and classify pixels based on inputs (imagery and training data). Since the algorithm is a "black box," the researcher may examine the inputs and outputs. GEE has a number of machine learning classifiers that may be used for both supervised and unsupervised classification. Support Vector Machine, Classification and Regression Tree (CART) classifier, Random Forest, and Naive Bayes are common (Ayodele, 2010).

Support vector machine (SVM)

Support vector machine is a non-parametric machine learning classifier that is available in the Google Earth engine (Lin, 2015). As first proposed by (Vapnik, 1999), it is a classification algorithm based on statistical learning theory that is theoretically capable of catching crucial spectral signatures with only a few training samples, deriving the hyperplane to achieve reliable and satisfied land cover classification. The classification problem in support vector machines is tackled by determining the optimal interval

between distinct classes by finding the best hyperplane of the feature space (Haykin, 2008).

The hyperline of SVM is described in (Vapnik V. ,., 1999) by the following equations:

$$y_i(w_i + b) \geq 0 \ldots\ldots\ldots\ldots\ldots\ldots\ldots\ldots\ldots\ldots\ldots. \text{eq } 2.1$$

Where: y_i is the point lying on the boundary of the hyperplane, w_i is the weight vector, and b is called the bias.

Finally, (Haykin, 2008) concluded that "SVM classifiers provide an analytic approach for determining the optimum size of the feature (hidden) space, thereby ensuring the optimality of the classification task."

Many studies have demonstrated the capability of SVM in land cover mapping and suggest it would be an effective algorithm for deriving the change in land cover using 30-meter-resolution Landsat images. For example, a study conducted in Malaysia, Klang Valley, used an SVM classifier to classify satellite remotely sensed multispectral data. The study emphasized that SVM classified the land cover within the study area with high accuracy (Bahari, 2014).

A similar study in Mongolia effectively applied SVM for mapping the historical land use and land cover change as a result of the changing trend and type of features. The mapping was successfully done with the best performance capability of the SVM classifier, and the overall accuracy was very high (Jamsran, 2019).

(Shi & Yang, 2015), demonstrate the effectiveness of SVM for heterogeneous land cover mapping. The study found that SVM can significantly improve mapping accuracy, particularly for spectrally and spatially complex land cover categories. In addition to the mapping of LULC, SVM has been used for various purposes, for example, in ground water potential mapping (Naghibi & Dashtpagerdi, 2017), modeling low flow time series (Sahoo et al., 2019), and ground water quality evaluation (Chang et al., 2010).

All of the studies have found that SVM has strengths in terms of classification accuracy and training time. As a limitation, the studies suggested that the classification accuracy of SVM can be affected by the size and quality of the training sample.

Classification and regression tree (CART) classifier

CART is a sophisticated technique that uses a decision tree (DT) classification algorithm to build a decision tree from a collection of training data. The choice is made based on the attribute with the largest normalized information gain (Breiman, 1984).

CART's ability to handle both numerical and categorical data makes it easier to comprehend, visualize, and interpret the classified images (Herrera et al., 2019). Additionally, it differentiates the most significant variables from non-significant ones (Bittencourt & Clarke, 2003).

The CART classification algorithm repeatedly splits input data based on a statistical test to increase the similarity of the training data in the resulting node (Mondal, 2019). The main limitation of the CART algorithm is the presence of high variance across samples, which leads to high variability in predicting classes and estimates (Hayes, 2015).

Random forest classifier (RF)

RF is the most popularly applied machine learning classifier (Belgiu, 2016) and the most frequently used classifier on the GEE platform (Tamiminia, 2020). An RF classifier uses training data to classify statistical patterns in huge datasets and then selects the best classification for all pixels within the imagery using a succession of decision trees (Breiman L. , 2001). It's a non-parametric machine learning technique that uses multiple decision trees to categorize a random sample of training data using covariate predictors. The majority vote among all trees determines the final class and model development options. Because the effectiveness of a random forest classifier is not affected by the number of variables per split, the user can define the number of trees and variables per split in a random forest (Breiman L. F., 1984).

The random forest method has several advantages, such as more effective results for large datasets (Herrera, 2019). Can handle thousands of variables without reducing them (Rodriguez-Galiano, 2012) and gives an estimate of variables that are important in classification. It can produce unbiased estimates of generalization errors (Siroky, 2009) and is computationally lighter than other tree ensemble methods.

The accuracy of RF classification relies on two parameters, namely the number of trees (Ntree) and the number of features (Mtry). The classification accuracy of RF is more sensitive to Mtry than Ntree, where the smaller Mtry would shorten the processing time

but provide lower accuracy. It is common to set Ntree as large as possible; this will not affect the efficiency or cause overfitting during the classification process (Belgiu & Drăguţ, 2016).

Several studies have demonstrated the effectiveness of using the random forest classifier in LULC mapping. For instance, Nurfadila et al., (2019) used Sentinel 2 satellite data with a spatial resolution of 10 m to map land use and land cover change, resulting in more optimal LULC maps with a 95% overall accuracy. Moreover, this classifier has been widely used to classify satellite data for wetland mapping (Masoud, 2017), cropland mapping (Oliphant et al., 2019), and natural hazard susceptibility area mapping (Taalab et al., 2018).

Naive Bayes (NB)

The Bayesian theory of probability and predictions of the unknown class are used or applied by a naive Bayes classifier, which assumes that the features have substantial (naive) independence. This makes the Naive Bayes classifier a probabilistic model (Camargo et al., 2019). NB assumes that the feature class doesn't depend on the presence or absence of any other feature class; instead, it depends on the nature of the probability model, which makes the datasets train quicker (Ratika Pradhan, 2010).

The NB classifier was successfully deployed for gully erosion and landslide susceptibility assessment (Chen et al., 2019), Spatial Prediction of Groundwater Potentiality: Assessing the spatial likelihood of a flood hazard (Liu, 2016).

2.3.4 Image processing

Image processing is a method to perform some operations on an image in order to get an enhanced image or extract some useful information from it. It is a type of signal processing in which the input is an image and the output may be an image or characteristics or features associated with that image. In image processing, the preprocessing stage includes the detection and restoration of band lines, geometric rectification or image registration, radiometric calibration, atmospheric correction, and topographic correction. Accurate geometric rectification or image registration of remotely sensed data is a prerequisite for a combination of different source data in classification processes. The study would be done using Landsat imaginaries to identify changes in

LULC distribution in the watershed over a 26-year period from 1997 to 2022. To avoid seasonal variation and minimize cloud cover, the selection of dates for acquired data is made in the dry season and with the same annual season as the acquired years. To view and discriminate the surface features clearly, all the input satellite images would be composed using the RGB color composition.

Individual pixels on the images were used as validation units for the image accuracy assessment. User's, producer's, overall, and kappa coefficient assessments were done as part of the accuracy assessment. User's accuracy measures commission mistakes that correspond to pixels from other classes that the classifier has categorized as belonging to the class of interest (Rwanga and Nudambuki, 2017). The producer's assessment indicates the number of omission mistakes corresponding to pixels belonging to the class of interest that the classifier missed (Thapa and Murayama, 2009). The overall accuracy refers to the percentage of correctly classified samples (Story and Congalton, 1986). The kappa coefficient quantifies the proportionate reduction in error caused by a classification algorithm (Fahsi et al., 2000).

Kappa coefficient was calculated using Equation 2.2 (Congalton, 1991)

$$\text{kappa cofficinet (T)} = \frac{\left((\text{TS X TCS}) - \sum \llbracket((\text{CT X RT}))\rrbracket\right)}{\left(\text{TS2} - \sum \llbracket((\text{CT} - \text{RT}))\rrbracket\right)} - - - - - - - - eq\ 2.2$$

Where TS = Total Sample, TCS = Total Column Sample, CT = Column Total, RT = Row Total

2.3.5 Ground truth and classification accuracy assessment

A ground truth or field survey is done in order to observe and collect information about the actual condition on the ground at a test site or study area and determine the relationship between remotely sensed data and observed data. It is recommended to have the ground truth at the same time of data acquisition, or at least within the time that the environmental condition does not change.

Classification accuracy assessment is a general term for comparing the classification to geographical data that is assumed to be true to determine the accuracy of the classification process. Usually, the assumed true data is derived from ground truth. A set

of reference pixels is usually used. Reference pixels are points on the classified image for which actual data is known, and the reference pixel is randomly selected.

2.4   Hydrological modeling

Hydrological models are a relatively complex mathematical description of the hydrologic cycle (Linsley K., 1982). They define the actual physical processes of the hydrologic cycle and represent the behavior of the watershed in transforming a hydrologic input (rainfall) into an output (streamflow or runoff). Hydrological models are characterizations of the real-world system. The best model is one that produces outcomes that are as close to reality as possible while using the fewest number of parameters and having the least degree of model complexity (Gayathri et al., 2016). Streamflow models are therefore mathematical expressions that simulate streamflow or runoff like the way a watershed would operate on the same rainfall event. The model structure and architecture are determined by the objective for which the model is built (Singh & Woolhiser, 2002). There are many different reasons why modeling the rainfall-runoff processes of hydrology is required. The main reasons behind this are a limited range of hydrological measurement techniques and a limited range of measurements in space and time (Beven & Cloke, 2012). Therefore, it is necessary to develop a means of extrapolating from those available measurements in space and time to an ungauged watershed and into the future to assess the likely impact of future hydrological change. Hydrological models are characterizations of the real-world system. The researchers use a wide range of hydrological models; however, the applications of those models are highly dependent on the purposes for which the modeling is made. (Beven & Cloke, 2012). Stated that many rainfall-runoff models are carried out purely for research purposes as a means of enhancing knowledge about hydrological systems. He also adds that other types of models are developed and employed as tools for simulation and prediction, aiming ultimately to allow decision-makers to improve their decision-making about hydrological problems. Before developing the hydrological models, it is vital to understand how the watershed responds to rainfall under different conditions.

Based on the process description, the hydrological models can be classified into three main categories (Shaw, 1998).

Lumped model: in lumped models, the entire river basin is taken as a single unit where spatial variability is disregarded, and hence the outputs are generated without considering the spatial processes. The parameters often do not represent the physical features of hydrologic processes and usually involve a certain degree of empiricism.

Distributed models: parameters of distributed models are fully allowed to vary in space at the resolution chosen by the user. The distributed modeling approach attempts to incorporate data concerning the spatial distribution of parameters together with computational algorithms to evaluate the influence of this distribution on simulated precipitation runoff behavior. Distributed models generally require a large amount of data. (Beven & Cloke, 2012), explains that the distributed model does have some problems with its non-linearity, scale, uniqueness, and uncertainty.

Semi-distributed models: to overcome the difficulties of fully distributed, another semi-distributed model is a compromise between lumped and fully distributed. According to Moradkhani, (2008) the algorisms in semi-distributed conceptual models are simple but physically based. Parameters of semi-distributed models are partially allowed to vary in space by dividing the basin into several smaller sub-basins. The main advantage of these models is that their structure is more physically based than the structure of lumped models and requires fewer input data points than fully distributed models. SWAT, HEC-HMS, and HBV are considered semi-distributed models.

Watershed hydrologic models have been developed for many different reasons and, therefore, have many different forms. However, they are designed to meet one of the two primary objectives. The first objective of watershed modeling is to gain a better understanding of the hydrologic processes in a watershed and how changes in the watershed may affect these phenomena. The second one is the generation of synthetic sequences of hydrologic data for facility design or for use in forecasting. They are also providing valuable information for studying the potential impacts of changes in land use or climate.

Recently, hydrological simulation models, including SWAT, HEC-HMS, and others, have been developed partly to quantify the influence of changes in LULC and management practices on the hydrologic cycle. Moreover, with the development of the

GIS and RS methods, the hydrological catchment models have been more physically based and distributed to enumerate various interactive hydrological processes considering spatial heterogeneity (Mohan & Shrestha, 2000).

2.4.1 Model selection criteria

The choice of the best model depends on the project objectives. The model must be evaluated and selected before being applied to estimate catchment output. The selection of a hydrological model should include the structure of the model, time setup, representation of the physical process, requirements for input data, and hardware or software (Nemec J, 1993).

Nowadays, there are different models used to predict the hydrology of a given watershed and also developed partly to quantify the influence of change in LULC and management practices on the hydrologic cycle. Hydrologiska Byråns Vattenbalansavdelning (HBV), SWAT (Arnold et al., 1998), Hydrologic Simulation Program Fortran (HSPF), MIK SHE (System Hydrologique European) (Butts M.B, 2005) Hydrologic Engineering Center's Hydrologic Modeling System (HEC-HMS) (Choudhari K, 2014) and TOP MODEL (Gayathri, 2015) are some of the models.

There are various criteria that can be used to choose the right hydrological model for a specific problem. These criteria are always project-dependent, since every project has its own specific requirements and needs. Further, some criteria are also user-dependent and subjective. Among the various project-dependent selection criteria, there are two fundamental ones that must always be answered:

➢ Required model outputs are important to the project and therefore to be estimated by the model (does the model predict the variables required by the project, such as the long-term sequence of flow?) (Cunderlik, 2003),

➢ Hydrologic processes that need to be modeled to estimate the desired outputs adequately (is the model capable of simulating single-event or continuous processes?), (Cunderlik, 2003),

➢ Availability of input data (can all the inputs required by the model be provided within the time and cost constraints of the project?) (Cunderlik, 2003) ,

- ➢ Price (does the investment appear to be meaningful for the objectives of the project?) (Cunderlik, 2003),
- ➢ The model must be able to simulate agricultural areas because the study area can be classified as an agricultural watershed (Birhanu D, 2009),
- ➢ The ability of a hydrological model to integrate GIS for hydrologic data development, special model layers and interfaces (Kassa.T, 2009),
- ➢ The model must be ready and freely available, both for researchers and for future use in the country.

Based on the above criteria and to meet the objectives of this study, a semi-distributed SWAT model is selected. The model includes a set of mathematical descriptions of the hydrologic cycle, and they are based on a set of interrelated equations that try to convert the physical laws that govern extremely complex natural phenomena into abstract mathematical forms.

2.4.2 Reasons for selecting SWAT model

The reasons behind selecting the SWAT model for this study are:
- ➢ The model was applied for land use and land cover change impact assessment in different parts of the world.
- ➢ The model simulates the major hydrological processes in the watersheds.
- ➢ It is less demanding on input data, and
- ➢ It is readily and freely available.

SWAT is a semi-distributed, physically based, continuous-time, widely used, and flexible modeling tool that addresses many aspects of catchment (Thomas C, 2015). One of the main advantages of SWAT is that it can be used to model watersheds with less monitoring data (Geremew, 2013). The SWAT model has gained international acceptance as an inter-disciplinary watershed modeling tool by many international SWAT conferences (Gassman et al., 2007), and can be downloaded freely from http://swat.tamu.edu/software. The interface of the SWAT model is compatible with Arc-GIS, which can integrate many available geospatial data points to accurately represent the characteristics of the watershed (Geremew, 2013).

Weather variables for computing the hydrologic balance in SWAT are precipitation, maximum and minimum temperature, solar radiation, wind speed, and relative humidity. Daily inputs can be entered directly, or the weather generator can be used to simulate daily values for these variables. The weather generator can be downloaded from the SWAT web site http://swat.tamu.edu/software other than these DEMs (Digital Elevation Models), soil map, a land use map is also needed for the model.

A major limitation to large-area hydrologic modeling of SWAT is the spatial detail required to correctly simulate environmental processes. For example, it is difficult to capture the spatial variability associated with precipitation within a watershed. Another limitation is that data files can be difficult to manipulate and can contain several missing records. The model simulations can only be as accurate as the input data. The other limitation is that the SWAT model does not simulate detailed event-based flood and sediment (Geremew, 2013).

To achieve the objectives of LULC change and its impacts on streamflow in Kiltie River, the following selection criteria are considered for selecting the type of model to be used:

➢ The SWAT model predicts the output in an acceptable range to meet the objective of the study.

➢ Availability of input data.

➢ Technical support: What documentation is available about the model? Ease-of-use, and it is readily and freely available.

Based on the above selection criteria, the SWAT model is selected for detailed analysis and investigation of LULC change effects on streamflow in the Kiltie watershed.

2.4.3 Application of SWAT model in impact study

The SWAT model is used to analyze the impacts of land use change on discharge, erosion, sedimentation, and water quality in gauged and ungauged watersheds. The special feature of SWAT is the use of HRUs, where designated land use, soil type, and slope information can be grouped into a file for each subwatershed. Outputs at the HRU level are aggregated at the subwatershed level and eventually delivered from upstream to downstream subwatersheds via channel routing (Arnold et al., 1998). On the other hand,

users can assign one HRU per subwatershed so that the SWAT project will be closer to a physical-based model with modern computer technology.

The SWAT model has been applied in agricultural watersheds and has been successfully calibrated and validated in many areas of the world. SAWT has been applied globally to various subjects, including LULC change (Shiferaw et al. 2018). The study indicates that the SWAT model is capable of simulating the hydrologic process in the complex and data-poor watershed with reasonable model performance statistical values. (Getachew & Melesse, 2012) applied the SWAT model of Lake Tana Reservoir Water Balance and reported that the overall model performance was satisfactory. Similarly, Tibebe, (2011) also applied the SWAT model to evaluate surface runoff generation and soil erosion rate for a small watershed (Keleta Watershed) in the Awash River basin, Ethiopia, and recommended that the SWAT model provide a useful tool for soil erosion assessment in the watershed and facilitate planning for sustainable land management.

2.5   Previous studies on the impact of LULC change on streamflow

In Ethiopia, studies showed that LULC change affected streamflow and hydrological cycle process in different basins, sub-basins, and catchments (Dibaba et al. 2020a; Assefa et al. 2022). For instance, a studie of Hassen (2022) in Baro Basin indicated that converting forests, shrubs, and grasslands into agricultural lands affects the river's streamflow and evapotranspiration. Late et al. (2021) extrapolated that for the period 2019-2050, surface runoff increased by 4.23 percent during the short rain season and 2.0 percent during the dry season due to LULC alterations in the Nashe watershed of Blue Nile Basin. Cultivated land enhances streamflow throughout the major rain season and decrease evapotranspiration, but there is unpredictability during the short rainy and dry seasons (Adnan and Atkinson 2011; Hyandye et al. 2018). In Northwestern Ethiopia, according to Dibaba et al. (2020b), agricultural land expanded by 16 percent over the last 30 years, while forest land areas decreased by 12 percent.

Andualem & Gebremariam (2015) studied the LULC change of the Gilgel Abay watershed, Abay Basin, using ERDAS Imagine 2014 and analyzed the discharge of the river using SWAT modeling. According to his results during the 25 year study period (1986 - 2011), most parts of the grassland and shrub land were converted to cultivated

land. An increase in cultivated land by 33.79% resulted in an increase in streamflow by 5.87 m3/s.

The result of Geremew, (2013) in the Gilgel Abay watershed, Lake Tana basin, used (RS) and (GIS) integrated with the SWAT model for the assessment of the impacts of land cover changes on streamflow showed that the cultivated land has expanded during the study period of 1986 – 2001. Using the two generated land cover maps, two SWAT models were set up to evaluate the impacts of land use and cover changes on the streamflow of the study watershed. The Nash-Sutcliff efficiency and coefficient of determination (R^2) were used for evaluating the model's performance. The surface discharge increased, while groundwater discharge decreased from 1986 to 2001 due to the increase in cultivated lands. The model results showed that the streamflow characteristics changed due to the land cover changes during the study period.

Getachew & Melesse, (2012), analyzed the land cover change between 1985 and 2011 in the Angereb watershed and the effect of these changes on the runoff and reservoir inflows in the watershed. The SWAT model was used to investigate the impact of land cover change on streamflow. Land cover change analysis has shown that cultivated land and built-up areas have increased while forest and grass land have decreased between 1985 and 2011. The evaluation of the SWAT model response to the land cover has shown that the mean wet monthly flow for the 2011 land cover increased by 39% compared to the 1985 land cover. On the other hand, dry average monthly flow decreased by 46% in 2011 compared to 1985 land cover.

3 METHODOLOGY

3.1 Description of the study area

3.1.1 Location and topography

The study area is found in the northern part of Ethiopia, Amhara Region, which is geographically located between $11^0 10$' and 11^0 28' N latitude and 36^0 50' and 36^0 57' E longitude. As shown in the Figure 3.1 below, the watershed is found in the Tana sub-basin and which is one of the Gilgel Abay sub-watersheds, and the river drains to the northern part of the Gilge Abay River. The altitude ranges from 1829 to 2667 m. The area of the Kiltie watershed is around 598.67 km^2. The main rainy season is from June to September.
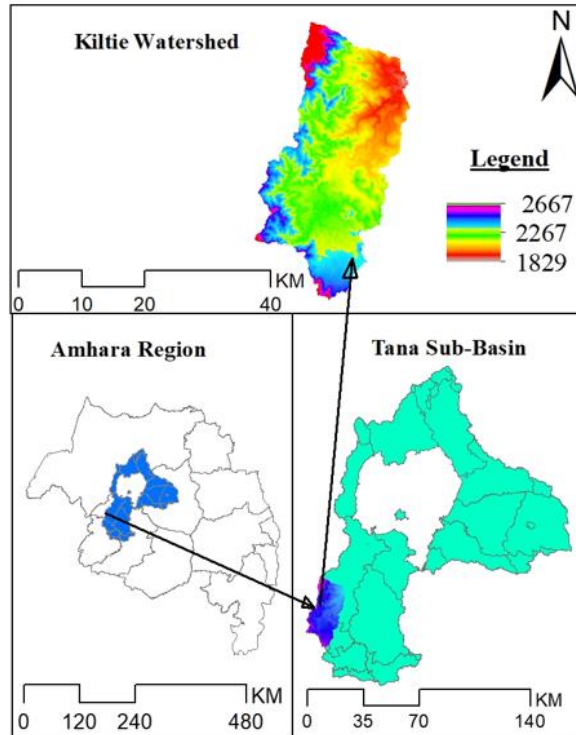
Figure 3.1 Location map of the study area including topographic map

Topography is defined by the digital elevation model (DEM), which describes the elevation of any point in a given area at a specific spatial resolution as a digital file. The northwest and southwest parts of the Kiltie watershed have elevation characteristics of mountainous landscapes. The peak elevation within the watershed is 2667 masl, and the minimum elevation, which is found in the north-east part of the watershed, is 1829 masl.

3.1.2 Climate of the study area

According to the traditional climate classification of Ethiopia, the study area was classified in the Woina Dega climatic zone. The study area annual rainfall ranges from 1344 mm to 2047 mm and mean annual rainfall of the study watershed is 1677mm. The main rainfall season, which accounts for more than 70% of the annual rainfall distributions of the study area occurs from June to September. The monthly rainfall distributions of the study area indicate that July and August are the wettest months of the year in all the selected stations. The mean maximum temperature is 25.4^0C and mean minimum temperature is 9.7^0C.

3.2 Methods of data collection

The impact of land use and land cover on streamflow in the Kiltie watershed has been evaluated using the SWAT model. For the completion of this study, primary and secondary data were used. In watershed modeling, the quality and quantity of acquired data have a great effect on the performance of the model. Particularly, the SWAT model requires good quality that includes DEM, soil, land use and land cover data, streamflow, and climatic data. Generally, the data are mainly classified into two main categories: spatial and time-series data.

3.2.1 Spatial data

DEM is an important spatial input acquiring from the ASTER Global Digital Elevation Model (ASTER-GDEM) obtained from USGS earth explorer for the automatic extraction of topographic parameters for the soil and water assessment tool (SWAT). Topography is defined by a DEM that describes the elevation of any point in a given area at a specific spatial resolution. So, DEM data is important for the hydrological modeling of a watershed. Therefore, in this study, DEM data with 30 m resolution in raster format is used and projected to the Universal Transverse Mercator (UTM) on the spheroidal of WGS84 to correct the errors and fit into the model requirements.

LULC data is very essential for SWAT input to determine the watershed characteristics and for a comparison of the impacts of LULC change on the streamflow of the watershed. Therefore, detailed analysis and mapping of LULC are critical for proper hydrological modeling. The LULC map and all datasets from 1997–2022 were generated from the Google Earth Engine platform. Dry seasons were selected to get good quality (free of cloud cover) of satellite images and making it easy to identify the classified land use.

The soil data of the watershed was obtained from the Amhara Design and Supervision Work Enterprise as classified shape file. These shape file is used for the determination of the available dominant soil types in the study area using ArcGIS 10.8 software.

The satellite imagery used in this study to classify LULC changes is the Landsat_5 Thematic Mapper (TM) for the year 1997, the Landsat_7 Enhanced Thematic Mapper for the year 2010, and the Sentinel_2 for the year 2022 from the United States Geological Survey (USGS). Each of them is analyzed individually, and change detection analysis is done by performing pre and post-change detection techniques.

3.2.2 Time series data

To simulate the hydrological condition of the watershed, the SWAT model needs hydrological and metrological datasets. The main metrological datasets used were daily precipitation, maximum and minimum temperature, relative humidity, wind speed, solar radiation, and sunshine hour, which were obtained from the National Meteorological Institute of Ethiopia (NMIE) with a different record length of the year. Those data were collected from the north-west Metrological institute of Ethiopia. The metrological stations used for this study are shown in (Table 3.1).

Table 3.1: Metrological stations location used for the study

No	Station Name	Latitude	Longitude	Elevation	Record Length
1	Dangila	1264817.961	264988.171	2116	1997 - 2022
2	Injibara	1216262.141	272648.022	2568	1997 - 2022
3	Wottet Abay	1257614.475	286364.103	1920	1997 - 2022

For performing sensitivity analysis, calibration, and validation of the model, streamflow data is required. Hydrological data like the observed daily streamflow of the Kiltie River, which covers a period of 1997–2003, were obtained from the Abay Basin Authority.

3.2.3 Collection of training data

The primary data were collected at filed which was used for further analysis, interpretation and comparison and expressing watershed characteristics. The data that were collected at field using GPS for selected LULC and other relevant data for this study. The collected ground truth data were used as training points for supervised classification, accuracy assessment and geometric correction of satellite images of the watershed. A minimum of 35 and a maximum of 50 ground control points had been collected from the field for each of the classified LULC classes. In order to minimize the impact of the location of the sample points on the classification results, we tried to maintain most of the sample points at the same location all over the 26-year study period, unless land use change was identified visually during the sample point selection.

Figure 3.2: Collection of training data

For the collection of sample data for land cover type, the target area is clipped, and the true color composite and false color composite methods are used for the extraction of spectral and special features from Landsat images based on the pixel-based approach. This helps to select training points effectively for each of the land cover types in the study area. The selected sample points were imported into the GEE script to run the classification.

3.2.4   Required Software and materials

Table 3.2: Software tools and materials used in this study

No	Materials	Version	Purpose of the material
1	ArcGIS	10.8	Preparation of study area map and data processing
2	Google Earth Engine		For land use land cover map processing and preparation
3	Google earth pro		For investigating historical images of the study area
4	GPS	GARMIN	For the collection of ground truth points
5	MS excel	2013	For data analysis
6	SWAT	2012	River discharge simulation
7	SWAT-CUP	5.1.6	Sensitivity analysis, calibration and validation

3.3   Data analysis and quality checking

3.4   Filling missing rainfall data

In some metrological stations, missing data occurs due to instrumental or personal errors. Filling in missing data is very important for hydrology analysis and simulations using data from long-term series. Thus data from the surrounding gauges are used to estimate

the missed rainfall data. There are different methods for filling in missing rainfall data from those arithmetic mean and normal ratio methods used in this study.

The average annual rainfall at each of these three index stations differs within 10% of the average annual rainfall of the station X (the station with missing data), the arithmetic mean method can be used to fill in the missed value. The station average method for estimating missing data uses n gauges from a region to estimate the missing point rainfall Px.

$$Px = \frac{1}{N}\sum_{i=1}^{n} Pi -------------- eq\ 3.1$$

Where Px is missed rainfall value, Pi in rainfall at gauge i, and N is number of nearby gauging stations.

On the other hand, the average annual rainfall at each of these three index stations differs by more than 10%, the normal ratio approach is applied.

$$\% \text{ difference} = \frac{Nx - Ni}{Nx} ----------eq\ 3.2$$

Nx –Ni must be positive. Then, the mean of the nearby station difference is determined.

$$Px = \frac{Nx}{m} * (\frac{P1}{N1} + \frac{P2}{N2} + ------\frac{Pm}{Nm}) --------eq\ 3.3$$

Where Px is the missing data at station x, Nx is the missing data station normal annual rainfall, Nm normal annual rainfall at station m and m is number of nearby gauges.

In this study, the arithmetic mean of the entire period was used to fill in the missed values for the station with less than 10% missed recorded, and the normal ratio approach was applied to calculate the missed data values before the data was used by the model.

3.4.1   Consistency of rainfall data

Consistency and continuity of rainfall data series are very important for obtaining reliable results from such studies. Different factors could affect the consistency of rainfall records at a given station. Among the factors:

- ➢ Damage and replacement of a rain gauge
- ➢ Change the gauge location or elevation.
- ➢ Growth of high vegetation or construction of buildings
- ➢ Change in measurement procedure

➢ Human, mechanical, or electrical error in taking readings

The Double Mass Curve (DMC) is used to check the quality, homogeneity, and consistency of rainfall, as well as adjust inconsistent data. This technique is based on the principle that when each recorded piece of data comes from the same parent population, it is consistent. The procedure consists of comparing the accumulated annual precipitation at the station in question with the accumulated annual precipitation for a group of surrounding stations. The scatter plot is drawn between the interested gauge and a number of surrounding gauges.

The existence of a break in the double mass curve indicates a change occurred in that year. Adjusting the data to the condition before change is equivalent to bringing the observed point on the line after the change vertically to the line that is the extension of the line before the break. If the slope of the line prior to the change is m1, and the slope after the change is m2, then the adjustment factor will be m1/m2. The multiplier will be applied to the post-change observed data to obtain the adjusted data. According to the double mass curve, in this study, at all gauging stations, the observed precipitation data shows homogeneity.
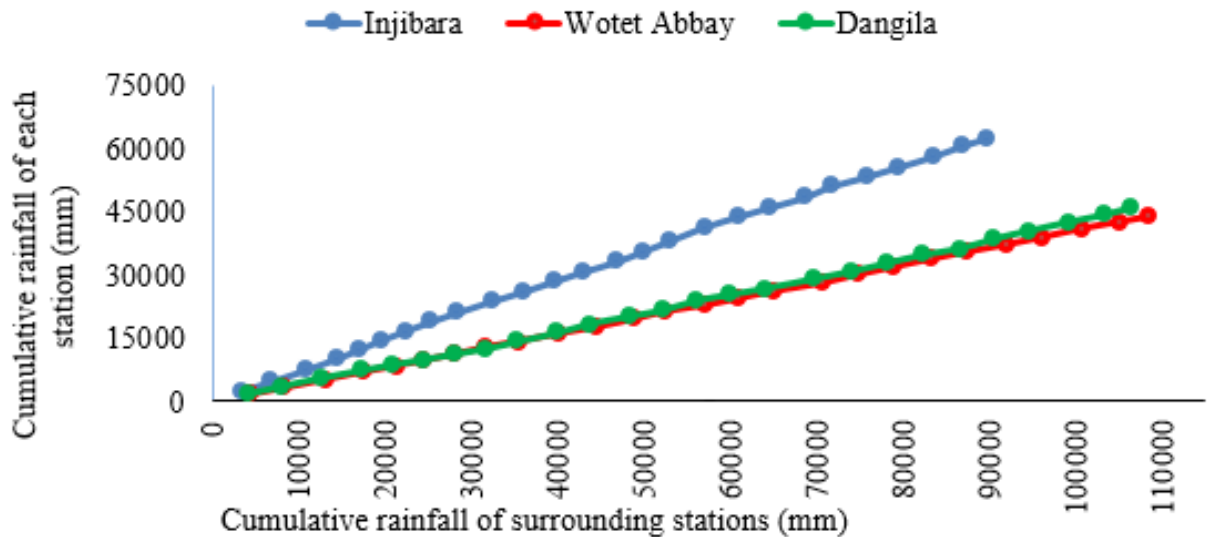
Figure 3.3 Double Mass Curve

3.5 Land use land cover change analysis

Google Earth Engine (GEE), a JavaScript Application Program Interface (API), is used to analyze the spatial and temporal land use and land cover dynamics. JavaScript API codes are taken from https://earthengine.google.org/. However, the script is customized for the present usage study area. Landsat satellite images are contained in Google Earth Engine's public data archive and can be used to detect and estimate the long-term dynamic of land use and land cover changes. The application of GEE greatly reduces the analysis time by utilizing Google's distributed computing infrastructure platform. This study uses annual composite Landsat Surface Reflectance images covering an area of around 598.67 km^2 of the Kiltie watershed, for classification and further analysis. Three annual different images from three different Landsat series are used in this study. When selecting the right type of dataset, several aspects have to be considered; the most important are the availability, accessibility, and quality of the data.

Table 3.3 Landsat images used for LULC change analysis

Landsat Images	Path	Row	Sensor	Resolution/ Scale	Number of bands	Date of acquisition	Cloud cover
Landsat 5	170	52	TM	30	7	03/01/1997	0.00
Landsat 7	170	52	ETM	30	8	03/01/2010	0.00
Sentinel-2	170	52	S1	10	13	01/01/2022	0.00

A large number of high-quality samples are selected by visual interpretation (for the year 2022), and Google Earth images (for others) are used for selecting training samples to improve the classification accuracy. Four popular machine-learning algorithms of Support Vector Machine (SVM), Classification and Regression Tree (CART), Random Forest (RF), and Naive Bayes are used to identify and map long-term LULC change.

The Landsat archived data from the (USGS) collection was loaded as an image collection, and the selected study area was injected into the GEE and displayed. The LULC classification technique is applied and evaluated by developing code on the GEE platform using the supervised classification method and Landsat imagery for each selected year.

3.5.1   Image preprocessing in GEE

To minimize confusion and overcome timeout errors, three customized GEE code editor scripts are used for each individual year separately. Each of the individual year images passes the following main components of image preprocessing:

3.5.1.1   Accruing Landsat surface reflectance image collection

The first step is accessing and accruing data, which is started by a function to call and make a composite image by calling a series of images from the image collections.

3.5.1.2   Image cloud removal

After acquiring the required image collections, the next step is injecting the shape file of the study area into the Google Earth Engine platform in the form of a zip file format or other options for a selected year. The Landsat image collection is loaded by filtering the date of acquisition and this is done to minimize the effect of the rainy season on the classification result. Then, a cloud-masking function is developed by assigning a cloud score to each pixel in the image collections for the removal of cloud covers. For this a cloud threshold of 1% and 5% is selected based on the visual interpretation of Landsat imagery. This cloud masking function computes a cloud likelihood score to compare multiple views of the same point for relative cloud likelihood, and pixels with a cloud score higher than 1% and 5% are screened out. The filtered image collections are acquired after the cloud mask, and a limited date and year range are applied.

Figure 3.4: Cloud free image of the study area in GEE

3.5.2 Image classification

In the study, Landsat and Sentinel satellite images were used to identify changes in land use and land cover distribution in the Kiltie watershed over 26 years from 1997 to 2022. Three images were selected for the time period for land cover mapping of the watershed. During this time period, different years are selected to represent the land cover conditions of the year.

The obtained images are then classified within the GEE using the Random Forest (RF) classifier with the following six land cover categories: agriculture land, forest cover, grass land, built-up area, barre land, and shrub land. Finally, the relevant results from the analysis, such as charts, images, maps, and tables from the classified images, are exported to Google drive.

3.5.3 Land use and land cover change using different GEE classifiers

In this study, four machine learning algorithms that were used for LULC classification were evaluated and compared. These classifiers are: Random Forest, Support Vector Machine, CART, and Naïve Bayes. However, the accuracy and performance of these classifiers were evaluated according to ground truth points. In case of the Kiltie Watershed ground truth points were collected (150) for all LULC site on the year 2022. The recent and free cloud cover Sentinel-2 image that was collected on the dates of 2022-03-01 (https://earthengine.google.com) was used to classify and evaluate the algorithms in LULC classification for the Kiltie watershed.

In this study, six land use and land cover categories (agricultural land, forest land, grass land, shrub land, barre land, and built-up area) have been detected and collected using the pixel-based approach.

3.5.4 Method of accuracy assessment

Accuracy assessment helps to understand how precise the maps are to use the data accurately and effectively. Failure to attain the expected target levels of precision is commonly interpreted as a lack of satellite data classification against LULC. Various algorithms accuracy was evaluated using metrics obtained from error matrix, such as Overall Accuracy (OA), Producer Accuracy (PA), Consumer Accuracy (CA), and Kappa

Coefficient (KC) (Abdi, 2020; Foody, 2002). Below, equations are used for acquiring accuracy.

Overall accuracy = Total number of correct sample – total number of samples ------- eq 3.4

Producer Accuracy = 100% - error of omissions ----------------- eq 3.5

Consumer Accuracy = 100% - error of commissions --------------- eq 3.6

$$\text{kappa cofficinet } = \frac{\left((\text{TS X TCS}) - \sum[(\text{CT X RT})]\right)}{\left(\text{TS2} - \sum[(\text{CT} - \text{RT})]\right)} - - - - - - - - eq \text{ 3.7}$$

Where TS = Total Sample, TCS = Total Column Sample, CT = Column Total, RT = Row Total

3.5.5 Land use land cover data processing

The land use and land cover are processed and generated by the Google Earth Engine. Among the classified classes of land use and land cover, the dominant land cover is identified, and the generated land use and land cover is converted to SWAT database code for the running of the SWAT model.

Table 3.4: Original and redefined land use and land cover name of the Kiltie Watershed

Original land use land cover	Redefined land use land cover according to SWAT database	SWAT code
Agriculture land	Agricultural land closely grown	AGRC
Forest cover	Forest Evergreen	FRSE
Urban area	Residential-High Density	URHD
Barre land	Range Brush	BARR
Grass land	Range Grasses	RNGE
Shrub land	Range Brush	REGB

3.5.6 LULC change detection

The importance of change detection is to determine which land use class is changing to another. The most commonly used land use change detection methods include image overly, classification comparison of land cover statistics, change vector analysis, principal component analysis, image rationing, and the differencing of the normalized difference vegetation index (NDVI). The process of identifying differences in LULC change in the Kiltie watershed would be done by observing the classified images at

different times. Therefore, comparisons based on three satellite images are made. In this study, a classification comparison of land cover statistics is used. The direction of changes (positive or negative) in each land cover type is determined by comparing the land cover area at various periods.

3.6   Hydrological modeling

River flow data is required for performing sensitivity analysis, calibration, and validation of the model. There is no active hydrometric station within or at the outlet of the Kiltie watershed, but there is a short period of records (7 years) that is from 1997 to 2003. For this study, two-thirds of 7 years of flow data was used for calibration and the one-third is for validation, while one year data was used for the warm-up period.

3.6.1   SWAT model description

SWAT model was developed by United States Department of Agriculture-Agriculture Research Service (USDA-ARS). It is a conceptual model that functions on a continuous time step. Model components include weather, hydrology, erosion/sedimentation, plant growth, nutrients, pesticides, agricultural management, channel routing, and pond/reservoir routing. SWAT model is a semi-distributed parameter model that operates on a daily time step so as to predict the impact of management measures on flow, sediment and agricultural chemical yields of the watersheds (Getachew & Melesse, 2012). SWAT applies physical algorithm to estimate the runoff using biophysical data such as precipitation, soil properties, topography, land use and land cover, and SCS curve number equation (Zare et al., 2016). SWAT is a physically based semi-distributed continuous time-scale hydrological model, which works on a daily time step. This model can simulate runoff, sediment, nutrients, pesticide, and bacterial transport from agricultural watersheds. It simulates the hydrological cycle parameters based on the water balance represented in equation within the watershed (Neitsch, 2005). The model estimates relevant hydrologic components such as evapotranspiration, surface run-off and peak rate of run-off, ground water flow and sediment yield for each HRUs unit. SWAT is fixed in GIS interface. Arc-SWAT ArcGIS extension is a graphical user interface for the SWAT 2005 involved from AVSWAT which is an ArcView extension developed for an earlier version of SWAT. In SWAT the watershed is divided in to multiple sub

watersheds, which are then further subdivided into Hydrologic Response Units (HRUs). HRUs are used to describe spatial heterogeneity in terms of land covers, soil types and slope classes within a watershed.

3.6.2 Hydrologic component of SWAT model

The simulation of hydrology in the watershed was conducted in two separate divisions. The first stage was the land phase of the hydrologic cycle that controls the amount of water, sediment, nutrient, and pesticide loadings to the main channel in each sub-basin. The second division was routing phase of the hydrologic cycle that can be defined as the movement of water, sediment, nutrient, and organic chemicals through the channel network of the watershed to the outlet.

3.6.2.1 Land phase

In land phase the hydrologic cycle, SWAT simulates the hydrological cycle based on the water balance equation:-

$$\text{SWt} = \text{SWo} + \sum_{i=1}^{t}(\text{Pday} - \text{Qsurf} - \text{Ea} - \text{Wseep} - \text{Qgw}) \; - - - - - - \text{eq 3.8}$$

Where, SWt is the final soil water content (mm), SWo is the initial soil water content on day i (mm), t is the time (days), Pday is the amount of precipitation on day i (mm), Qsurf is the amount of surface runoff on day i (mm), Ea is the amount of evapotranspiration on day i (mm), Wseep is the amount of water entering the vadose zone from the soil profile on day i (mm), and Qgw is the amount of return flow on a day i (mm).

SWAT operates on daily climatic data and is used to predict the impact of LULC on streamflow. In the SWAT model, a watershed is divided into multiple sub-watersheds, which is further divided into Hydrologic Response Unit (HRU) which consists of homogeneous LULC, topographical, and soil characteristics. The HRU is represented as a percentage of the sub-watershed area. The water balance components of each HRU are computed on the daily time step. Water balance is the driving force behind all the processes in the SWAT model. Weather data such as daily precipitation, maximum and minimum temperature, solar radiation, wind speed, and relative humidity are used to do the water balance by SWAT model. The model has eight major components: hydrology,

weather, sedimentation, soil temperature, crop growth, nutrients, pesticides, and agricultural management Neitsch, (2005).

3.6.2.2 Surface runoff

Surface runoff occurs whenever the rate of precipitation exceeds the rate of infiltration. Runoff in SWAT can be estimated either Soil Conservation Service (SCS) Curve Number (CN) method (Service, 1972) or the Green and Ampt infiltration method (Green, 1911). The lateral method is better in estimating run off volume precisely; its sub daily time step data requirement makes it difficult to be used for the cause of our country. In this study Soil Conservation Service (SCS) method was selected because it used to estimate surface runoff for small agricultural watersheds and the Curve Number (CN) varies non-linearly with the moisture content of the soil. It drops to zero as the soil approaches the wilting point and increases to be near 100 as the soil approaches saturation, with higher CNs associated with higher runoff potential watershed. This method is widely used J. G. Arnold, (1998).

According to USDA-SCS, 1985, mathematically expressed SCS curve number equation is:

$$Qs = \frac{(Pa - Ia)^2}{Pa - Ia + s} - - - - - - - - - - - eq\ 3.9$$

The above equation is functional for Pa > Ia, on the other hand Qs = 0 for Pa < Ia.

Where Qs is the accumulated runoff (mm), Pa is the rainfall depth for the day (mm), and Ia is infiltration to the soil for the day (mm). The retention parameter S, defined by equation:

$$S = 25.4 * \left(\frac{100}{CN - 10}\right) - - - - - - - - - - - - eq\ 3.10$$

Where CN is the curve number for the day and its value is the function of land use practice, soil permeability and soil hydrologic group.

The initial abstraction, Ia, is commonly approximated as 0.2S and surface runoff becomes:

$$Qs = \frac{(Pa - Ia)^2}{(Pa + 0.8S)} - - - - - - - - - - - - - eq\ 3.11$$

For the definition of hydrological groups, the model uses the U.S Natural Resource Conservation Service (NRCS) classification. The classification defines a hydrological group as a group of soils having similar runoff potential under similar storm and land cover conditions. Thus, soils are classified in to four hydrologic groups (A, B, C, and D) based on infiltration which represent high, moderate, slow, and very slow infiltration rates, respectively.

3.6.3   SWAT model setup

This study uses Arc SWAT 2012 to generate a hydrologic model for streamflow from the study watershed, Kiltie, at a GIS interface. Arc SWAT is an extension of Arc GIS, and its toolbar is added to Arc GIS for use to meet the objective of the study. The SWAT model passes three key processing steps: watershed delineation, hydrological response unit (HRU) analysis, and weather data definition. In the SWAT model simulation part, sensitivity analysis of parameters, and calibration and validation of the model was done.

3.6.3.1   Watershed delineation

The primary steps in creating a new SWAT model project, in addition to the preparation of input data is watershed delineation from DEM. The watershed delineation involves five major steps: DEM set-up, stream definition, outlet definition, and watershed outlet selection and definition. Watershed delineation is performed using DEM at 30 m resolution. Watershed delineation is more developed in the section by defining the outlet point for the whole watershed. The outlet location of the Kiltie watershed is added manually to the defined streamline. The final step in the delineation of the watershed is the calculation of basin parameters such as geomorphic parameters and stream reach. The size of the sub-basin in the watershed would affect the assumption of homogeneity. In this study, the delineation of the watershed has been done, and the watershed outlet is manually added and selected to finalize the watershed delineation. With this information, the model automatically delineates the watershed into sub-watersheds for simulation.

3.6.3.2   Hydraulic Response Unit

After performing the automatic watershed delineation, the watershed is partitioned into a hydrological response unit and lumped land areas within the sub-watershed, which incorporates the same land use, soil, and management practices. LULC, soil, and slope

characterization for watersheds are performed using commands from the HRU analysis menu of the Arc SWAT toolbar. This tool is used to load the LULC and soil layers of the study area watershed. Therefore, LULC/soil/slope combinations and distribution for the delineated Kiltie watershed are determined in HRU analysis. Finally, the watershed is divided into HRUs, which have similar soil, LULC, and slope combinations. Any parcel of land within one sub-watershed that shares the same combination of those three features land use, soil, and management practices would be considered one HRU.

The prepared composite LULC map and soil map are given as input to the model in this step. The lookup table containing various SWAT LULC class codes is prepared. This prepared lookup table is linked to the SWAT LULC database. These lookup tables have two columns named value and name. The value in the lookup table corresponds to the value of LULC in the attribute table for the classified image, and the name corresponds to the name of the LULC class, which corresponds to the name in the SWAT database.
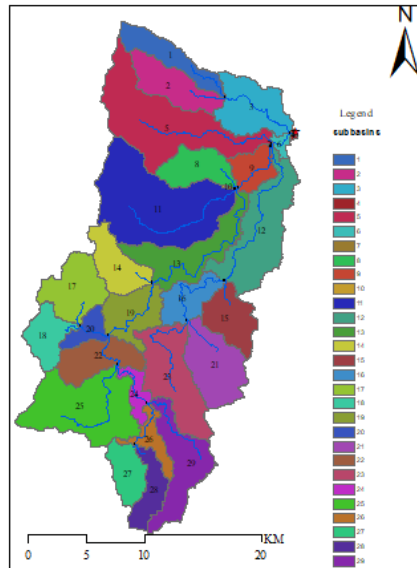
Figure 3.5: hydrological response unit (HRU) map of the Kiltie watershed.

3.6.3.3   Weather data definition

SWAT requires a long-term daily record of precipitation, solar radiation, wind speed, relative humidity, and maximum and minimum temperature. The SWAT weather generator model is used to fill in missing weather data values. Since in the study area most of the stations have no full weather data, like relative humidity, solar radiation, and wind speed data, by selecting one synoptic station that has full weather data, SWAT

generates the above data by using a weather generator. For this reason, Dangila station is a synoptic station that has full weather data and generates data for the other station. The Penman-Monteith method, which utilizes relative humidity, wind speed, and solar radiation data records, is employed for the estimation of potential evapotranspiration (PET). The weather generator collects all information about climate data in one folder, and from this, the data has been imported into the SWAT 2012 model database.

The last step before a SWAT simulation is going to be run is to write all of the input files required by SWAT and produce them from the prepossessed data from Arc SWAT. Once they are written, individual files can be edited through Arc SWAT.

3.6.4 Model simulation

After the model set up, the next step is running the model for monthly time step from 1997 to 2022. The output result cannot be used for further analysis without evaluating the ability of the model to predict streamflow through sensitivity analysis, model calibration, and validation.

3.6.5 SWAT Calibration and Uncertainty Procedure (SWAT-CUP)

SWAT-CUP is a computer program designed to integrate various calibration/uncertainty analysis programs for SWAT using the same interface. The program links SUFI-2, PSO, GLUE, ParaSol, and MCMC procedures to SWAT. It enables sensitivity analysis, calibration, validation, and uncertainty analysis of SWAT model (Neitsch et al., 2011). The program guides the input files necessary for running a calibration program. Each SWAT-CUP project contains one calibration method and allows running the procedure many times until convergence is reached. It allows saving calibration iterations in the iteration history for later use.

Prediction uncertainty arises from the uncertainty parameters, the model, and the input. In the concept of SUFI-2, all these uncertainties are assigned to the parameter distributions (Abbaspour K.C, 2014). The increasing of the uncertainties in the parameters leads to uncertainties in the model output variables, which are expressed as the 95% probability distributions. These are calculated at the 2.5% and 97.5% levels of the cumulative distribution of an output variable generated by the propagation of the parameter

uncertainties using Latin hypercube sampling. This is referred to as the 95% prediction uncertainty or 95PPU (Abbaspour K.C, 2015).

3.6.6 Sensitivity analysis

Sensitivity analysis is the process of determining the rate of change in model output with respect to changes in model input (parameters). It is necessary to identify key parameters and the parameter precision required for calibration (Zhan, 2013). Sensitivity analysis is an integral part of model development and involves the analytical examination of input parameters to help in model validation and provide guidance for further research. Sensitivity analysis is used to identify how much variation in input values for a given variable impacts the results of a mathematical model. It identifies the data to be collected for analysis to evaluate a project's investment. SWAT model is used in this study and the sensitivity analysis of simulated streamflow for the watershed were performed using the monthly observed flow for identification of sensitive parameters and for further calibration of the simulated streamflow using the Sequential Uncertainty Fitting Version 2 (SUFI-2) program.

The first step of the calibration and validation process in SWAT is the determination of the most sensitive parameters for a given watershed. Sensitivity analysis is performed on the SWAT model to identify influential parameters in the modeled streamflow to avoid the problem of overparameterization. The importance of sensitivity analysis was to allow the reduction of a number of parameters that must be estimated by reducing the computational time required for model calibration. Once the sensitive analysis is done, calibration can be performed for a limited number of influential parameters. To improve simulation results and thus understand the behavior of the hydrologic system in the study area watershed, sensitivity analyses are conducted using the entire flow parameters for the SWAT model. Therefore, sensitivity analysis is used as an instrument for the assessment of the input parameters concerning their impact on model output.

The current version of the SWAT model, SWAT 2012, provides algorithmic techniques for sensitivity analysis. Two types of sensitivity analysis are allowed when using (SUFI-2). Those are global sensitivity and one-at-a-time sensitivity analysis. The two above-mentioned sensitivity analysis methods may yield different results since the sensitivity of

one parameter depends on the value of other related parameters. In this study, global sensitivity analyses are performed, and the ranking of the parameters is determined.

3.6.7 Model calibration and validation

Model calibration is an interactive exercise used to get the most suitable parameters for modeling. Calibration and uncertainty analysis of the distributed watershed model is best done with some issues that deserve the attention and careful consideration of researchers. It involves the identification of the most important model parameters and changing the parameter set. The calibration is done on month-time setups using the average streamflow of the Kiltie River. After the model is calibrated and gets acceptable results, it is validated using data from the average monthly streamflow.

Validation is done to compare the model outputs with an independent dataset that is set for the calibration process without making further adjustments to the parameter values. The process continues until the simulation of the validation period of the stream confirms best the measured data of its correspondence so that the model performs satisfactorily.

In this study, the calibration and validation are performed in the SWAT calibration and uncertainty program (SWAT-CUP) 2012, version 5.1.6.2, which facilitates the calibration process. SWAT-CUP is a computer program for the calibration and validation of SWAT models. It is a public domain program and, as such, may be used and copied freely. The program links many algorithms SUFI-2 (Sequential Uncertainty Fitting Algorithm), PSO (Particle Swarm Optimization), MCMC (Markov Chain Monte Carlo), GLUE (Generalized Likelihood Uncertainty Estimation), and Parasol (Parameter Solution) to SWAT. A sequential uncertainty-fitting algorithm, referred to as SUFI-2, is used for uncertainty analysis.

Identifying parameters that do or do not have any significant influence on the model simulation is crucial not only in reducing parameter uncertainty but also in reducing overparameterization of the model, which can destroy its physical representation.

3.6.8 Model performance evaluation

To evaluate the model simulation outputs relative to the observed data, a model performance evaluation is necessary. Model performance is carried out to verify the

robustness of the model to simulate hydrological processes. There are various methods to evaluate the model's performance during calibration and validation periods.

Nash and Sutcliffe simulation efficiency (NSE) indicates the degree of fitness of observed and simulated data, and it is calculated using the following equation:

$$NSE = 1 - \frac{\sum_{i=0}^{N}(Qobs - Qsimu)^2}{\sum_{i=0}^{N}(Qobs - Qm, obs)^2} -------- eq\ 3.12$$

Where N is the number of compared values, Qobs is the observed data, Qm is the observed mean, and Qsim is the simulated data.

The NSE indicates how well the plot of the observed versus simulated value fits the 1:1 line. The closer the model efficiency to 1, the more accurate the model, and if it is found between 0 and 1, it indicates deviations between measured and predicted values. If NSE is negative, predictions are poor, and the average value of output is a better estimate than the model prediction.

The coefficient of determination (R^2) is an indicator of the extent to which the model explains the total variance in the observed data. It measures the ability of a model to predict or explain an outcome in a linear regression setting.

According to Moriasi et al., (2007), simulation judged as satisfactory if $R^2 \geq 0.6$ for flow.

$$R^2 = \frac{\sum(Xi - Xave)(Yi - Yave)}{\sqrt{(\sum(Xi - Xave)^2(Yi - Yave)^2)}} ----------- eq\ 3.13$$

Where *Xi* is the measured value, *X*ave is the average measured value, *Yi* is the simulated value, and *Y*ave is the average simulated value.

Percent bias (PBIAS) measures the average tendency of the simulated data to be larger or smaller than the observed counterparts. The optimal value of percent bias is 0, with low magnitude values indicating accurate model simulation. A positive value indicates model underestimation bias, and a negative value indicates model overestimation bias. PBIAS is computed as shown below.

$$PBIAS = \frac{\sum_{i=1}^{n}(Oi - Si)}{\sum_{i=1}^{n}(Oi)} * 100 ----------eq\ 3.14$$

Where, PBIAS is the deviation of the data being evaluated, expressed as a percentage Oi is observed discharge, and Si simulated discharge.

If PBIAS ± 25% for streamflow the model simulation can be judged as satisfactory.

The remote mean square error observation standard deviation ratio (RSR) incorporates the benefits of error index statics and includes a scaling and normalizing factor so that the resulting static and reported values can apply to various constituencies. RSR varies from the optimal value of "0," which indicates zero root mean square error or residual variation, and from the perfect model simulation to a large positive value. Generally, if the value of RSR is $\leq$ 0.70, the model simulation can be considered satisfactory.

$$\text{RSR} = \frac{\text{RMSE}}{\text{STDEVods}} = \frac{\sqrt{\sum_{i=1}^{n}(Oi - Si)^2}}{\sqrt{\sum_{i=1}^{n}(Oi - Savr)^2}} - - - - - - - -eq\ 3.15$$

Where, STDEVods is standard deviation of observed flow and Savr is simulated average flow.

Table 3.5 : Performance rating Moriasi et al., (2007)

Performance rating	RSR	NSE	PBIAS% Streamflow
Very good	0.00 < RSR < 0.50	0.75 < NSE < 1.00	PBIAS < ± 10
Good	0.50 < RSR < 0.60	0.65 < NSE <0.75	± 10 < PBIAS < ± 15
Satisfactory	0.60 < RSR <0.70	0.50 < NSE < 0.65	± 15 < PBIAS < ±25
Unsatisfactory	RSR > 0.70	NSE < 0.50	PBIAS > ± 25

3.6.9 Evaluation of Streamflow due to LULC changes

The impact of LULC change evaluation on streamflow is one of the most significant parts of the study. The study would be carried out for three different years. The three classified LULC maps, soil, climate, and streamflow data values would be used to evaluate the impact of land use and land cover change on streamflow. To evaluate the variability of streamflow due to LULC change, the three LULC maps will be used independently and in simulations while keeping other variables constant. After processing, the result discover annual variation and seasonal variation of streamflow due to the LULC map. Moreover, the general workflow is shown in Figure 3.7 below.
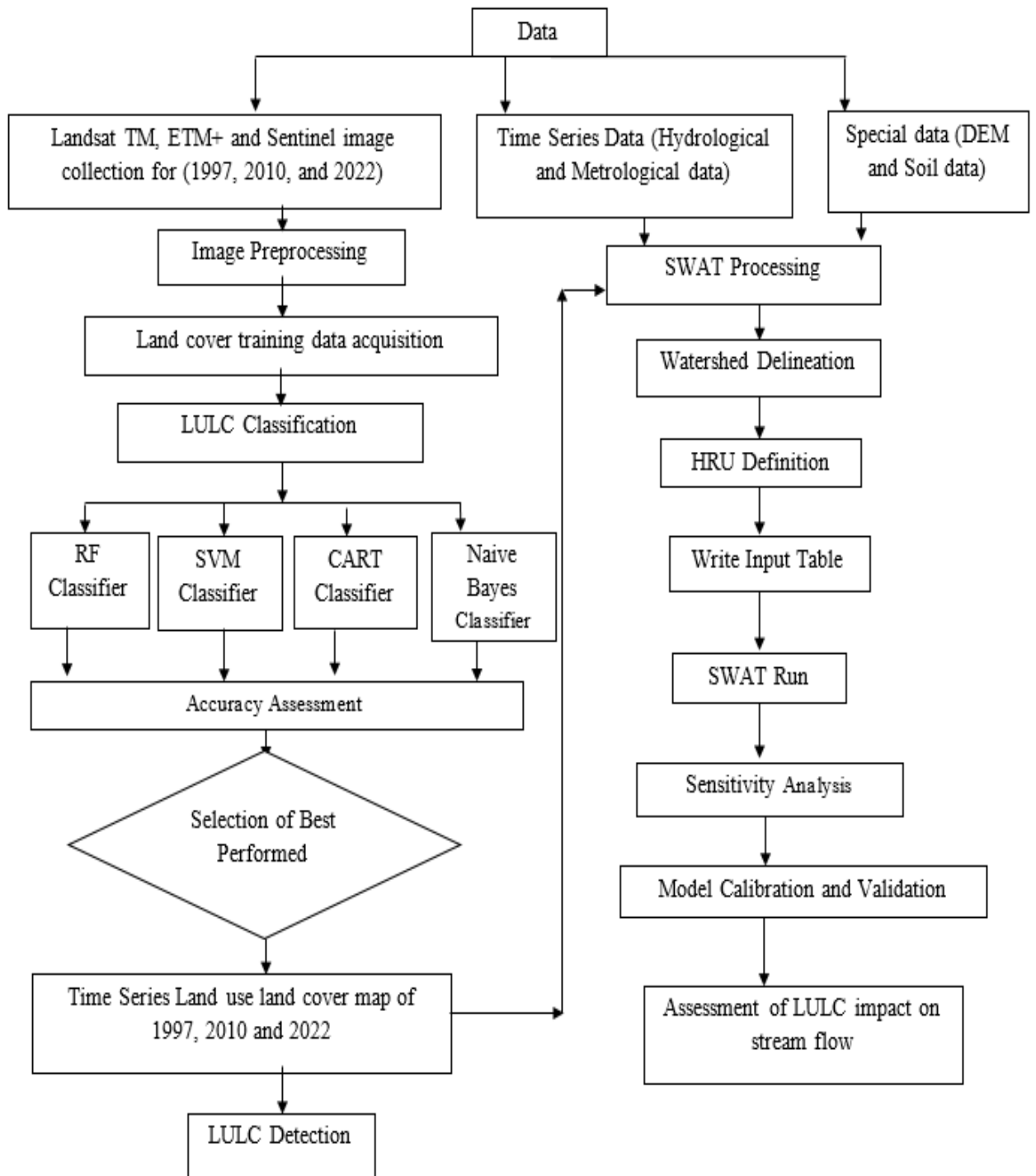
Figure 3.6: General work flow of the study

4   RESULT AND DISCUSSION

4.1   Land use and land cover change detection

4.1.1   Accuracy assessment

The error matrix, which is commonly applied to evaluate the accuracy of algorithms and select methods that were used for LULC classification, is applied in the study. However, in the LULC classification, the best-performed algorithm is presented in Table 4.1 below. From the four machine learning algorithms, the one that performed better in detecting the LULC map according to validation accuracy in the case of the Kiltie watershed was selected to generate a historical LULC map for 1997 and 2010.

Table 4.1: Summary of overall accuracy and kappa value for all algorithms in the year of 2022

Classifier	Over all accuracy %	Kappa value %
Random Forest	90.03	89.54
CART	80.66	78.3
Support Vector Machine	79.75	57.45
Fast Naive Bayes	71.90	38.32

In the case of the RF algorithm, the user's accuracy ranged from 81.67% to 95.00%, and it indicates the urban area detected as having 95% accuracy, whereas the producer's accuracy ranged from 75.38% to 98.155%. The algorithm was highly performed and better at detecting forest land with 98.15% of the producer's accuracy. A high commission error was observed in the agriculture land due to some of the agriculture land pixels laid on the other land features. The reason for the lower accuracy for these classes may be the larger size of the feature areas as well as the high distribution of agricultural land relative to other land covers. This might confuse the algorithms in differentiating the agricultural land from the other land. The overall accuracy of the algorithms for validation performance was 90.03%, and the statistical kappa coefficient value was 89.54%.

The LULC map are not very useful without a numerical statement about their accuracy. The RF algorithm accuracy of the map for the year 2022 is presented as an error matrix below in (Table 4.2) and for other periods it is described in **Appendices B.** The numbers

along the diagonal of the matrix indicate the number of reference pixels that are accurately

classified by the algorithm. The value outside the diagonal shows misclassification. As shown in (Table 4.2), the algorithm had difficulties during the classification of some of the land use and land cover features.

For example, grass land pixels were classified as agricultural land, urban area, barre land, and shrub land were classified as forest land and grass land because of the reflectance similarity of agricultural land with urban area and barre land and shrub land with forest land, grass land uses land cover types. In addition to this, among other land use land cover classes, more of the agricultural cover classes fall under the grass land class. This indicates that the algorithm has been confused in detecting the agricultural land class, grass land cover class, shrub land class, and forest land class. For the map of 2022, the overall accuracy was 90.03% and the kappa coefficient was 89.54%. This indicates that the algorithm ranged as very good (Taati et al., 2015).

Table 4.2: Summary of the Confused Matrix for the RF Algorithm for 2022

	Agriculture	Forest	Grass	Urban	Shrub	Barre land	sum	User Accuracy (%)	Commission Error (%)
Agriculture	49	0	11	0	0	0	60	81.67	18.33
Forest	1	53	0	1	1	0	56	94.64	5.36
Grass	4	0	49	1	0	1	55	89.09	10.91
Urban	2	0	0	57	0	1	60	95.00	5.00
Shrub	0	1	3	0	46	0	50	92.00	8.00
Barre land	4	0	2	0	0	44	50	88.00	12.00
Sum	60	54	65	59	47	46			
Procedure Accuracy (%)	81.67	98.15	75.38	96.61	97.87	95.65			
Commission Error (%)	18.33	1.85	24.62	3.39	2.13	4.35			

In the CART algorithm, the user accuracy ranged from 69.09% to 95.00%. Urban areas have about 95% user accuracy with a commission error of 5%. On the other hand, urban areas have a producer accuracy of 91.94% with an 8.06% omission error. In this classifier, a high commission error of about 30.91% has been observed at grass land because more of the grass land pixels are classified as agriculture land, as well as some of the other land feature classes. The overall accuracy was 80.66%, and the kappa value was 78.3%. This classifier shows less performance when compared to the RF classifier. The complete error matrix of this classifier is found in **Appendices B.**

In the SVM algorithm, the user accuracy ranged from 98.21% to 29.09%. Forest and agriculture land has about 98.21% user accuracy with a commission error of 1.79%. On the other hand, barre land has a producer accuracy of 97.56% with a 2.44% omission error. In this classifier, a high commission error of about 70.91% has been observed at grass land because more of the grass land pixels are classified as agricultural land, as well as some are lied on in the other land feature classes. The overall accuracy was 79.75%, and the kappa value was 45.57%. The complete error matrix of this classifier is found in **Appendices C.**

Finally, with the Naïve Bayes algorithm, the percentage of user accuracy ranged from 98% to 40%. Barre Land has about 98% user accuracy with a commission error of 2%. On the other hand, urban areas have a producer accuracy of 96.43% with a 3.57% omission error. In this classifier, a high commission error of about 60% has been observed at grassland because more of the barre land pixels are classified as agriculture, compared to the other land feature classes. The overall accuracy was 71.9%, and the kappa value was 38.32%. The complete error matrix of this classifier is found in **Appendices E.**

4.1.2   Land use land cover change

Change detection of the Kiltie watershed for 26 years was performed based on the previous LULC classification result of time series data. The (Figure 4.1) below shows, the LULC map of the Kiltie watershed for the year 1997, 2010, and 2022 that have been generated from image collection LANDSAT/LTO5/C2/T1_L2, LANDSAT/LE07/C2/T1/_L2, and COPERNICUS/S2_SR, respectively.

As shown in the (Figure 4.1) below, in the year 1997, most of the south-west and north parts of the study area were covered by grassland, and most of the middle and east parts were covered by agricultural land. On the other hand, a built-up area was covered on the southern part of the watershed. Barre land, forest land, and shrub land cover as little as the whole area of the watershed.

In case of this study during the year 2010, agricultural land area increased all over the watershed relative to the past land use class, built-up area, and barre land area slightly increased on the north part of the watershed when compared with the year 1997. In the upper part of the watershed, barre land slightly expands with the reduction of grass land and shrub land. Generally, agricultural land covers expand more than the whole watershed.

Finally, in 2022, there would be an expansion of agriculture land over the watershed. In addition to this, the barre land, forest cover, and built-up area increased to some extent. Whereas grass land and shrub land cover decreases relative to the past year classification. In the study area watershed forest cover increase from year to year because of the afforestation of Eucalyptus (Table 4.3).

According to Getachew and Melesse (2012), agricultural land and Built-up area increases during the study period of 1985 to 2011 on Angereb watershed. The expansion of cultivated land at the expanse of forest, shrub land and grass land in Gilgel Abay watershed between 1986 and 2019 periods is aligned with many studies in Ethiopian Highlands (e.g., Gashaw et al., 2017; Woldesenbet et al., 2017; Berihun et al., 2019). For example, Gashaw et al., (2017) has reported the expansion of cultivated land at the reduction of forest, shrub land and grass land in the Andassa watershed during 1985 – 2015 periods. There was also an increase of cultivated land and decrease of shrub land in the Lack Tana sub-basin between 1986 and 2010 periods (Woldesenbet et al., 2017). The area covered by natural vegetation showed was also decrease in Kasiry catchment (Upper Blue Nile Basin) during 1982-2017 periods (Berihun et al., 2019). Nigussie et al., (2017) has also indicated that the reduction of cultivated land in the Upper Blue Nile Basin between 2006 and 2017 periods was mainly attributed to the farmers growing interest in allocating more land to Acacia decurrens to remedy a decline in soil fertility and to provide fuelwood and charcoal.

In 1997, the land use land cover map (Figure 4.1 (A)) and the percentage cover of each land cover class indicated that the Kiltie watershed. In 2010, the land use land cover map (Figure 4.1 (B)) and the percentage cover of each land cover class showed that agriculture land increased by 11.44%, forest land increased by 0.01%, built-up area increased by 0.35%, grass land decreased by 8.46%, shrub land decreased by 6.05%, and barre land increased by 2.71% of the watershed. This year, agricultural land was expanded in most parts of the watershed. Similarly, 4.99% of agriculture land was dominantly increased, 3.98% of forest land was increased relative to the year 2010, 0.53% of built-up area was increased, and grass land cover decreased by 15.04% in the year 2022 (Figure 4.1 (C)).

The special analysis result of the land use dynamics was summarized as follows in the (Table 4.3) below. So that it is simple to compare land use land cover change patterns and the overall land use dynamics with time.

Table 4.3: Area coverage of each land use and land cover type

LULC Type	1997		2010		2022	
	Area (sq km)	Percentage	Area (sq km)	Percentage	Area (sq km)	Percentage
Agriculture land	287.89	48.09%	356.36	59.52%	386.22	64.51%
Forest cover	9.10	1.52%	9.15	1.53%	33.00	5.51%
Urban area	1.03	0.17%	3.11	0.52%	6.31	1.05%
Grass land	193.41	32.31%	142.79	23.85%	52.72	8.81%
Shrub land	102.76	17.16%	66.56	11.12%	94.16	15.73%
Barre land	4.48	0.75%	20.72	3.46%	26.28	4.39%
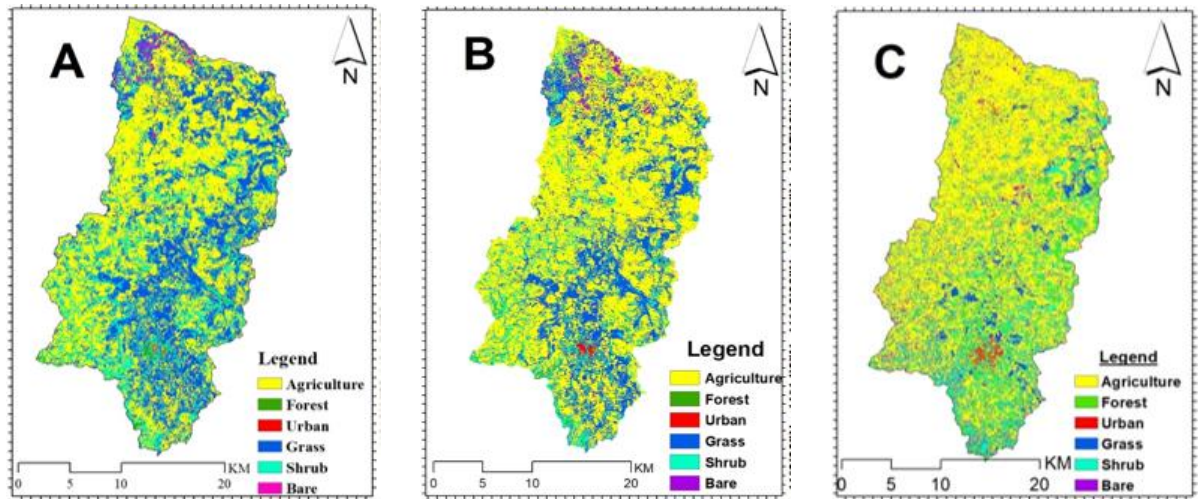
Figure 4.1: Classified LULC of the Kiltie watershed for A) 1997, B) 2010 and C) 2022.

4.1.3 Land use land cover change detection

A change detection map was produced for each class in the study area. Figure 4.1 shows the changed land use and land cover class of the study area, indicated with a variety of different colors. Table 4.4 below shows the change of one land use class to the other class coverage area and percentage by numerical value.

As shown in (Figure 4.2(A)), during the years 1997–2010, among the classified types of land use, land cover classes shrub land and grass land cover have decreased and been converted to agriculture land use. (Figure 4.2 (B)) describes the land use and land cover class of the years 2010–2022. During this period, more grass land and barre land were converted to agricultural land. Moreover, the grass land has been lost due to its conversion to agricultural land. Due to this trend, agriculture activity was very high during this period.

Finally, (Figure 4.2 (C)) shows major losses were noticed in grassland and barre land, whereas expansions were observed in agricultural land, urban area, and forest land covers. Generally, the analysis of LULC for the study watershed showed that agricultural land was predominant and showed a slightly continuous increment over the study period.
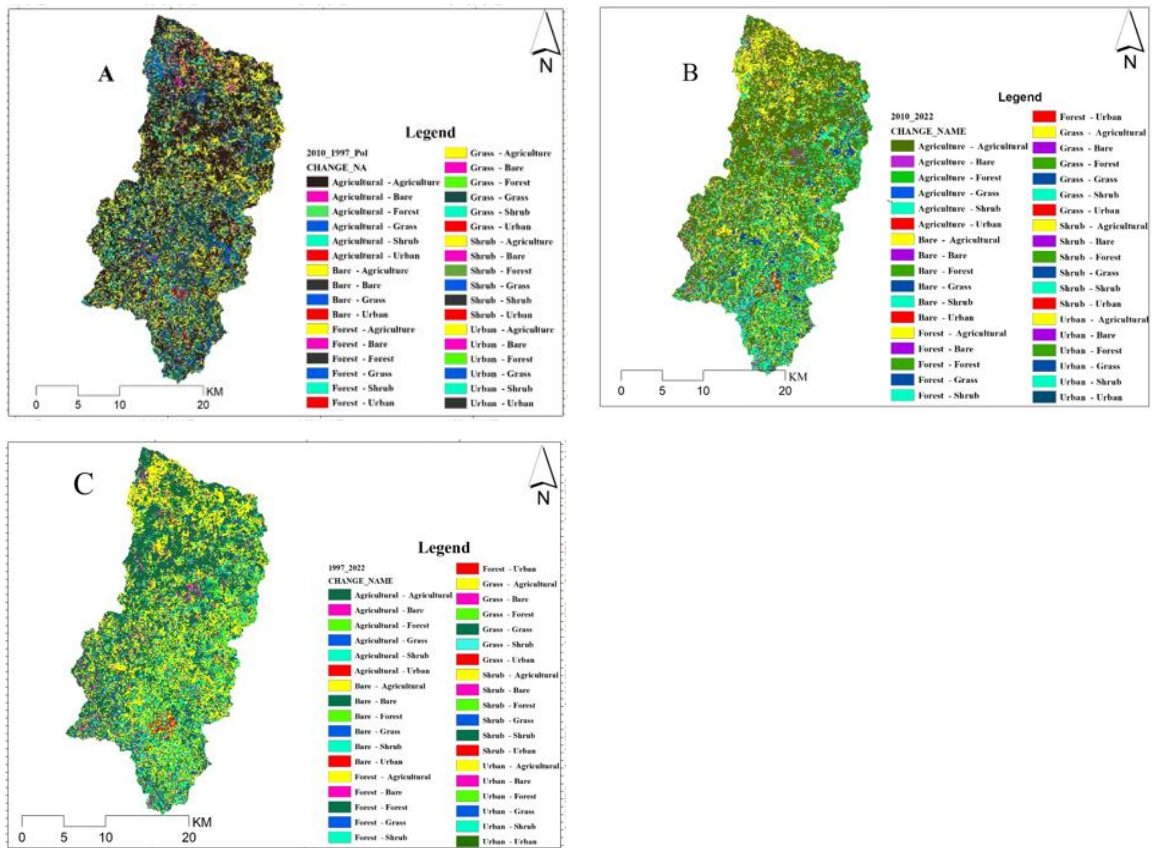
Figure 4.2: LULC change dynamics over A) 1997-2010, B) 2010-2022 and C) 1997-2022

Table 4.4: Major changes in LULC dynamics over the study period in Kiltie watershed

		1997 - 2010		2010 - 2022		1997 - 2022	
LULC	Change To	Area (Km^2)	%	Area (Km^2)	%	Area (Km^2)	%
Ag	Ag	231.93	80.57	262.80	73.76	214.78	74.62
	Ba	7.47	2.60	16.29	4.57	14.94	5.19
	Fr	1.60	0.56	13.85	3.89	10.03	3.49
	Gr	23.10	8.03	17.15	4.81	11.46	3.98
	Sh	22.68	7.88	43.55	12.22	34.81	12.09
	Ur	1.06	0.37	2.65	0.74	1.82	0.63
Ba	Ag	1.32	29.40	12.19	58.88	3.83	85.54
	Ba	2.16	48.30	2.04	9.83	0.53	11.91
	Fr	0.00	0.00	1.23	5.94	0.01	0.13
	Gr	0.99	22.16	1.24	5.99	0.05	1.11
	Sh	0.00	0.10	3.78	18.27	0.05	1.04

	Ur	0.00	0.06	0.23	1.11	0.01	0.27
Fr	Ag	0.40	4.37	1.71	18.76	2.15	23.67
	Ba	0.17	1.84	0.25	2.75	0.15	1.67
	Fr	3.08	33.89	2.83	31.01	2.45	26.96
	Gr	2.18	23.95	0.24	2.58	0.44	4.87
	Sh	3.11	34.19	4.01	43.92	3.49	38.40
	Ur	0.16	1.79	0.10	1.07	0.40	4.43
Gr	Ag	87.74	45.37	81.89	57.36	117.14	60.58
	Ba	5.13	2.65	3.06	2.14	5.28	2.73
	Fr	0.45	0.23	6.17	4.32	11.32	5.85
	Gr	89.45	46.26	29.51	20.67	31.20	16.13
	Sh	10.18	5.26	20.30	14.22	26.31	13.61
	Ur	0.43	0.22	1.85	1.30	2.13	1.10
Sh	Ag	34.65	33.73	26.12	39.26	47.87	46.59
	Ba	5.75	5.59	4.59	6.91	5.34	5.19
	Fr	3.99	3.88	8.80	13.22	9.13	8.89
	Gr	26.84	26.13	4.36	6.55	9.48	9.22
	Sh	30.43	29.62	22.01	33.07	29.26	28.48
	Ur	1.08	1.06	0.67	1.01	1.67	1.62
Ur	Ag	0.26	25.11	1.44	46.27	0.38	36.49
	Ba	0.04	3.55	0.04	1.39	0.03	2.63
	Fr	0.02	2.12	0.11	3.54	0.05	5.17
	Gr	0.20	19.28	0.22	7.17	0.08	8.01
	Sh	0.15	14.35	0.48	15.58	0.22	20.89
	Ur	0.36	35.38	0.81	25.98	0.27	26.59

AG = Agriculture, Fr = Forest, Ur = Urban, Gr = Grass, Sh = Shrub, and Ba = Barre

4.2 Streamflow evaluation

4.2.1 Sensitivity analysis of simulated streamflow

SWAT CUP 2012 is used for sensitivity analysis considering 25 flow related parameters to identify which model parameter is top sensitive that has a significant influence on controlling streamflow in Kiltie watershed. It was carried out for a period of seven years,

which includes both one-year warm-up periods from January 1, 1997, to December 31, 1997, the calibration period from January 1, 1998, to December 31, 2001, and validation periods from January 1, 2002, to December 31, 2003.

After the model simulation was done for 500 runs the result shows good fitting with the observed data (Figure 4.3) and all 25 selected parameters were reported as sensitive to different degree (**Appendices G**).
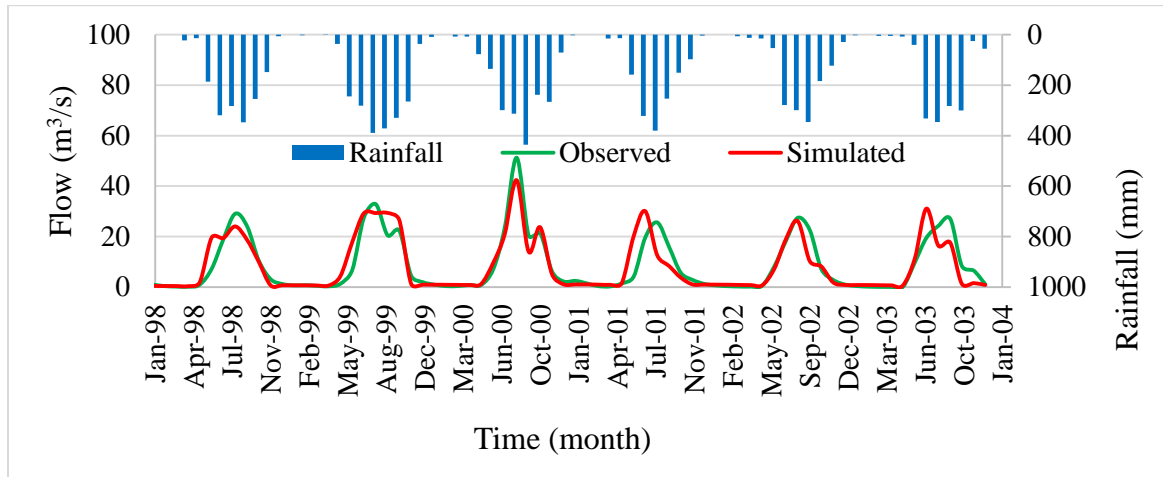
Figure 4.3: Best simulation for the year 1997

Out of the 25 flow parameters, only selected most top sensitive ones (Table 4.5) were identified for the model to avoid model overparameterization. The five most sensitive streamflow parameters from high to low sensitivity are CN2, CANMX, SOL_K ALPHA_BF, and EPCO. Table 4.5 shows the most top sensitive parameters for the 1997 year of LULC map. For the map of 2010 and 2022 the most sensitive parameters are presented in **Appendices H** and **Appendices I.** Figure 4.3 shows the best simulation for the beginning year that is 1997.

Table 4.5: Top 10 Sensitive Parameters for the LULC map of the year 1997

Parameters	t-stat	p-value	Rank
v_CN.mgt	13.967	0.0000	1
r_CANMX.hru	2.8217	0.0049	2
a_SOL_K.sol	2.7034	0.0071	3
v_ALPHA_BF.gw	2.3621	0.0185	4
a_EPCO.bsn	2.12926	0.0337	5
r_SOL_ALB.sol	1.78648	0.0746	6

v.HRU_SLP.hru	1.62168	0.1055	7
r_GW_DELAY.gw	1.4038	0.1610	8
r_TLAPS.sub	1.3673	0.1721	9
v_OV_N.hru	1.34589	0.1789	10

4.2.2 Calibration and validation

The graphical comparison of the observed and simulated streamflow during the calibration and validation periods are shown in Figure 4.4. Based on the performance rating value, the results of model performance during the calibration and validation periods of monthly streamflow demonstrated a good agreement between observed and simulated streamflow (Table 4.6) with the performance rating ranges: Coefficient of determination (R^2), Nash-Sutcliffe efficiency (NSE), PBIAS and RSR for the land use land cover map of 1997.

Table 4.6: Model Performance Measures for Calibration and Validation

Land use land cover map	Calibration				Validation			
	R^2	NSE	PBAS	RSR	R^2	NSE	PBAS	RSR
1997	0.83	0.83	3.4	0.42	0.8	0.77	8.9	0.48

The above Table 4.6 indicates the result of the simulation of the flow for the model performance that was adequately good during the calibration and validation periods. This indicates that the model performs well in simulating the generated streamflow from the watershed. Therefore, the simulation results can be used to assess the LULC impacts on streamflow. In addition to the above statistical measures, the following line graph (Figure 4.4) shows the relationship between observed and simulated streamflow during the calibration and validation of LULC maps for the years 1997. As we can see from the graph, there is a great relationship between observed and simulated streamflow. Therefore, the result of model performance (Table 4.6) indicates that SWAT model is a very good predictor of streamflow of the Kiltie watershed.
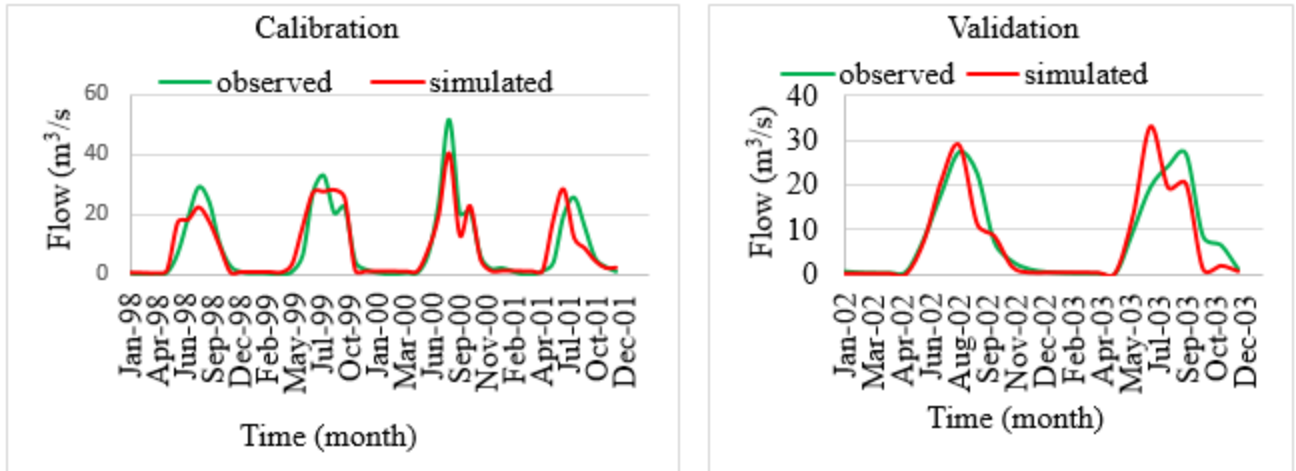
Figure 4.4: Model monthly calibration and validation for LULC 1997

4.3 Impact of land use land cover change on streamflow

4.3.1 Change of monthly streamflow

Table 4.7: Monthly Streamflow Change for the Study Period

Year	Jan	Feb	Mar	Apr	May	Jun	Jul	Aug	Sep	Oct	Nov	Dec
Obs	0.98	0.54	0.26	0.27	0.84	7.16	21.15	31.74	21.74	12.60	4.31	1.44
1997	0.92	0.91	0.84	0.80	1.43	12.49	24.60	24.78	16.16	12.15	1.94	1.02
2010	0.79	0.78	0.72	0.67	1.71	14.27	24.91	25.13	16.38	12.26	1.87	0.88
2022	0.77	0.76	0.70	0.66	1.24	12.22	25.16	25.38	16.61	12.37	1.87	0.85

By the year 1997, the average monthly flow was low relative to the year 2010. This is due to the effect of shrub land and grass land, which had good coverage on the watershed, about 17.16% and 32.31% of the watershed, respectively. The shrub land has ability to delay the runoff flow to the outlet of the watershed. However, the shrub was reduced by 6.04% in 2010 with a complete incensement of agricultural and barre land, and at the same time, the average annual streamflow was increased by 5,991,840 m^3. This indicates that the increase in agricultural activity and barre land class were responsible for the occurrence of this change in streamflow from the period 1997 to 2010. On the other hand,

58

during the period 2010–2022, a reduction in streamflow was noticed by 4,415,040 m³. At this period, the dominant land cover class was agricultural land and shows some increment on forest cover by 3.99% and the shrub land was also increased by 4.61% (Table 4.3). Forest and shrub land will delay the runoff to the outlet of the watershed and due to dominant land cover is agricultural land which uses more water because it has more porous media. In Figure 4.5 shows the model poorly predict stream flow in the month of June and July. This is happen because of the high porous media in the soil. (Figure 4.5) shows the monthly streamflow distribution over the study period.
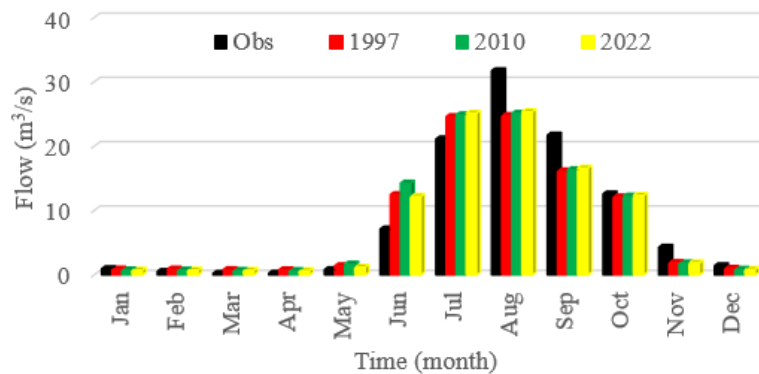
Figure 4.5: Monthly streamflow distribution throughout 1997 - 2022 (m³/s)

4.3.2 Change on seasonal streamflow

For the analysis of seasonal streamflow, the months of February, March, April, and May are considered Belg season, whereas June, July, August, and September are assigned as Kiremt season; additionally, the months of October, November, December, and January are assigned to Bega season.

The seasonal streamflow in (Table 4.8) shows variation throughout the three seasons because of LULC change. During Belg season, moderate decreases occurred between the years 1997–2010 and 2010–2022, by 259,200 m³/s and 1,347,840 m³. At the time, the smallest seasonal change was noticed in Bega season decrease by 601,344 m³ and increase by 155,520 m³. On the other hand, the effect of LULC change was largest in the Kiremt season increased by 0.665 m³/s and decreased by 0.330 m³/s, respectively. Generally during the study period, agricultural land, urban areas, and barre land increased continuously, while grass land and shrub land decreased throughout the year. This change in LULC increases the runoff in the watershed. On the other hand, forest cover increases throughout the year because of the afforestation activity of eucalyptus to provide

fuelwood and charcoal. This implies a streamflow decrease in the year 2022 in the Kiltie watershed which make delay of runoff at rein season.

Table 4.8: Seasonal mean streamflow (m^3)

	Belg season	Kiremt season	Bega season
1997	10316160	210681000	41554944
2010	10056960	217863000	40953600
2022	8709120	214299000	41109120

The significant change of streamflow were occurred in wet period than dry periods. During the wet season (June, July, August, September), the mean monthly flow was increased by 20,971,440 m^3 while the mean monthly flow decreased by 3,090,528 m^3 during dry season (October, November, December, January, February, March, April, May).

5   CONCLUSION AND RECOMMENDATIONS

5.1   Conclusions

LULC changes were detected periods between 1997 and 2022, in the cause of study area (Kiltie watershed). The LULC analysis clearly shows that grassland and shrub land were accompanied by an increase in agricultural land. This shows that agricultural activity within the watershed is very high, which, in turn, will affect the natural resources in particular and the hydrological cycle in general. The result in this paper shows that there has been a visible change in the LULC of Kiltie Watershed over the past years. Among the applied machine learning classifier algorithms, RF performed better, with the highest overall accuracy of 90.03% and a kappa coefficient of 0.895. The accuracy of the prepared land use and land cover was done using confusion matrixes, which measure the degree of agreement with the reference data. The value of all the accuracy indicators was within the acceptable range. Therefore, the accuracy of the three maps was found adequate to use the map for further analysis as per the objective of this thesis.

Streamflow for the watershed was determined from the SWAT model. The model is simulated for different land use and land cover maps; each map gives a different result, and the performance of the model has been perfectly measured using model evaluation statistics for each of the simulated streamflow. As a result of the LULC map of 1997, the NSE and R^2 values for the calibration period were 0.83 and 0.83, whereas for the validation period, the NSE was 0.77 and the R^2 0.80. All of the model performance measures described above were in the acceptable range, therefore the SWAT model has perfectly simulated the streamflow in Kiltie Watershed.

The average yearly streamflow of Kiltie watershed increased from 1997 to 2010 by 5,991,840 m^3, and from 2010 to 2022, the yearly streamflow was reduced by 4,415,040 m^3. The reduction in streamflow was due to a high percentage increase in agricultural land class, which have high porosity, and an increase in forest land class. For the study period between 1997 and 2022 in general, the streamflow was increased by 1,576,800 m^3 that shows the impact of LULC change in stream flow in the Kiltie watershed.

5.2   Recommendation

Based on the method and results obtained in this study, some recommendations were stated as follows:

- ➤ Due to significance of land use and land cover change, it needs effective participatory integrated watershed management.
- ➤ On the other hand, an increase in cultivated land and a reduction of shrub land and grass land were as a result of population growth, with a high interest in land partitioning for the purpose of agriculture activity for food security. This farming activity was not considered a soil water-absorbing property. It needs creating awareness about the farming practices and free grazing to increase the infiltration rate.
- ➤ The research was conducted by evaluating the effect of LULC changes on streamflow. So, further research of this kind can be computed based on the

assessment of the impact of LULC change on sediment transport, base flow, and ground water flow.

REFERENCE

Abate, A., & Lemenih, M. (2014). Detecting and quantifying land use/land cover dynamics in Nadda Asendabo Watershed, South Western Ethiopia. *International Journal of Environmental Sciences, 3*(1), 45-50.

Abbaspour, K. C., Rouholahnejad, E., Vaghefi, S., Srinivasan, R., Yang, H., & Kløve, B. (2015). A continental-scale hydrology and water quality model for Europe: Calibration and uncertainty of a high-resolution large-scale SWAT model. *Journal of hydrology, 524*, 733-752.

Abbaspour, K. C., Yang, J., Maximov, I., Siber, R., Bogner, K., Mieleitner, J., Zobrist, J., & Srinivasan, R. (2007). Modelling hydrology and water quality in the pre-alpine/alpine Thur watershed using SWAT. *Journal of hydrology, 333*(2-4), 413-430.

Akar, Ö., & Güngör, O. (2012). Classification of multispectral images using Random Forest algorithm. *Journal of Geodesy and Geoinformation, 1*(2), 105-112.

Andualem, T. G., & Gebremariam, B. (2015). Impact of land use land cover change on streamflow and sediment yield: a case study of Gilgel Abay watershed, Lake Tana sub-basin, Ethiopia. *Arba Minch University*.

Arnold, J. G., Srinivasan, R., Muttiah, R. S., & Williams, J. R. (1998). Large area hydrologic modeling and assessment part I: model development 1. *JAWRA Journal of the American Water Resources Association, 34*(1), 73-89.

Asitatikie, A. N. (2019). Impact of land use/land cover change on hydrology of the catchment: the case of upper Ribb catchment, lake tana sub basin, Ethiopia. *J Environ Earth Sci*.

Avand, M., Janizadeh, S., Naghibi, S. A., Pourghasemi, H. R., Khosrobeigi Bozchaloei, S., & Blaschke, T. (2019). A comparative assessment of random forest and k-nearest neighbor classifiers for gully erosion susceptibility mapping. *Water, 11*(10), 2076.

Ayodele, T. O. (2010). Types of machine learning algorithms. *New advances in machine learning, 3*, 19-48.

Bahari, N. I. S., Ahmad, A., & Aboobaider, B. M. (2014). Application of support vector machine for classification of multispectral data. IOP Conference Series: Earth and Environmental Science,

Belgiu, M., & Drăguţ, L. (2016). Random forest in remote sensing: A review of applications and future directions. *ISPRS journal of photogrammetry and remote sensing, 114*, 24-31.

Beven, K. J., & Cloke, H. L. (2012). Comment on: Hyperresolution global land surface modeling: Meeting a grand challenge for monitoring Earth's terrestrial water by Eric F Wood et al. *Water Resources Research, 48*(1).

Bittencourt, H. R., & Clarke, R. T. (2003). Use of classification and regression trees (CART) to classify remotely-sensed digital images. IGARSS 2003. 2003 IEEE International Geoscience and Remote Sensing Symposium. Proceedings (IEEE Cat. No. 03CH37477),

Bondelid, T. R., McCuen, R. H., & Jackson, T. J. (1982). Sensitivity of SCS models to curve number variation 1. *JAWRA Journal of the American Water Resources Association, 18*(1), 111-116.

Breiman, L., Friedman, J., Olshen, R., & Stone, C. (1984). Cart. *Classification and regression trees*.

Breiman, L. F. (1984). JH and Olshen. *RA Stone, CJ*.

Brook, H., Argaw, M., Sulaiman, H., & Abiye, T. A. (2015). The impact of land use/land cover change on hydrological components due to resettlement activity: SWAT model approach. *International Journal of Ecology and Environmental Sciences, 37*, 49-60.

Butts, M., Overgaard, J., Viaene, P., Dubicki, A., Strońska, K., & Szalinska, W. (2005). Flexible process-based hydrological modelling framework for flood forecasting–MIKE SHE. Proceedings of the International Conference Innovation, Advances and Implementation of Flood Forecasting Technology, Tromsø, Norway,

Camargo, F. F., Sano, E. E., Almeida, C. M., Mura, J. C., & Almeida, T. (2019). A comparative assessment of machine-learning techniques for land use and land cover classification of the Brazilian tropical savanna using ALOS-2/PALSAR-2 polarimetric images. *Remote sensing, 11*(13), 1600.

Chang, Y.-W., Hsieh, C.-J., Chang, K.-W., Ringgaard, M., & Lin, C.-J. (2010). Training and testing low-degree polynomial data mappings via linear SVM. *Journal of Machine Learning Research, 11*(4).

Choudhari, K., Panigrahi, B., & Paul, J. C. (2014). Simulation of rainfall-runoff process using HEC-HMS model for Balijore Nala watershed, Odisha, India. *International Journal of Geomatics and Geosciences, 5*(2), 253-265.

Cunderlik, J. (2003). *Hydrologic model selection for the CFCAS project: assessment of water resources risk and vulnerability to changing climatic conditions*. Department of Civil and Environmental Engineering, The University of Western ….

Dagnachew, M., Kebede, A., Moges, A., & Abebe, A. (2020). Land use land cover changes and its drivers in Gojeb River Catchment, Omo Gibe Basin, Ethiopia. *Journal of Agriculture and Environment for International Development (JAEID), 114*(1), 33-56.

Devia, G. K., Ganasri, B. P., & Dwarakish, G. S. (2015). A review on hydrological models. *Aquatic procedia, 4*, 1001-1007.

Di Gregorio, A. (2005). *Land cover classification system: classification concepts and user manual: LCCS* (Vol. 2). Food & Agriculture Org.

Dinka, M. O., & Chaka, D. D. (2019). Analysis of land use/land cover change in Adei watershed, Central Highlands of Ethiopia. *Journal of Water and Land Development*.

Drucker, H., Wu, D., & Vapnik, V. N. (1999). Support vector machines for spam categorization. *IEEE transactions on Neural Networks, 10*(5), 1048-1054.

Fentie, S. F., Jembere, K., Fekadu, E., & Wasie, D. (2020). Land use and land cover dynamics and properties of soils under different land uses in the tejibara watershed, Ethiopia. *The Scientific World Journal, 2020*, 1-12.

Flerchinger, G., Kustas, W., & Weltz, M. (1998). Simulating surface energy fluxes and radiometric surface temperatures for two arid vegetation communities using the SHAW model. *Journal of Applied Meteorology, 37*(5), 449-460.

Frank, R. T., Edmiston, M., Kendall, S. E., Najbauer, J., Cheung, C.-W., Kassa, T., Metz, M. Z., Kim, S. U., Glackin, C. A., & Wu, A. M. (2009). Neural stem cells as a novel platform for tumor-specific delivery of therapeutic antibodies. *PloS one, 4*(12), e8314.

Garg, V., Nikam, B. R., Thakur, P. K., Aggarwal, S. P., Gupta, P. K., & Srivastav, S. K. (2019). Human-induced land use land cover change and its impact on hydrology. *HydroResearch, 1*, 48-56.

Gassman, P. W., Reyes, M. R., Green, C. H., & Arnold, J. G. (2007). The soil and water assessment tool: historical development, applications, and future research directions. *Transactions of the ASABE,*

Gayathri, R., Murty, P., Bhaskaran, P. K., & Srinivasa Kumar, T. (2016). A numerical study of hypothetical storm surge and coastal inundation for AILA cyclone in the Bay of Bengal. *Environmental Fluid Mechanics, 16*, 429-452.

Genuer, R., Poggi, J.-M., & Tuleau-Malot, C. (2010). Variable selection using random forests. *Pattern recognition letters, 31*(14), 2225-2236.

Geremew, A. A. (2013). *Assessing the impacts of land use and land cover change on hydrology of watershed: a case study on Gigel-Abay Watershed, Lake Tana Basin, Ethiopia*

Gereta, E., Wolanski, E., & Chiombola, E. (2003). Assessment of the environmental, social and economic impacts on the Serengeti ecosystem of the developments in the Mara River catchment in Kenya. *Serengeti/Arusha, Tanzania*.

Getachew, H. E., & Melesse, A. M. (2012). The impact of land use change on the hydrology of the Angereb Watershed, Ethiopia. *International Journal of Water Sciences, 1*(6).

Getu Engida, T., Nigussie, T. A., Aneseyee, A. B., & Barnabas, J. (2021). Land Use/Land Cover Change Impact on Hydrological Process in the Upper Baro Basin, Ethiopia. *Applied and Environmental Soil Science, 2021*, 1-15.

Ghose, M., Pradhan, R., & Ghose, S. S. (2010). Decision tree classification of remotely sensed satellite data using spectral separability matrix. *International Journal of Advanced Computer Science and Applications, 1*(5).

Goldblatt, R., Rivera Ballesteros, A., & Burney, J. (2017). High spatial resolution visual band imagery outperforms medium resolution Spectral imagery for ecosystem assessment in the semi-arid Brazilian Sertão. *Remote sensing, 9*(12), 1336.

Gordon, L. J., Steffen, W., Jönsson, B. F., Folke, C., Falkenmark, M., & Johannessen, Å. (2005). Human modification of global water vapor flows from the land surface. *Proceedings of the National Academy of Sciences, 102*(21), 7612-7617.

Gorelick, N., Hancher, M., Dixon, M., Ilyushchenko, S., Thau, D., & Moore, R. (2017). Google Earth Engine: Planetary-scale geospatial analysis for everyone. *Remote sensing of Environment, 202*, 18-27.

Gumindoga, W. (2010). *Hydrologic impacts of Landuse change in the Upper Gilgel Abay River Basin, Ethiopia; TOPMODEL Application* University of Twente].

Gyamfi, C., Ndambuki, J. M., & Salim, R. W. (2016). Application of SWAT model to the Olifants Basin: calibration, validation and uncertainty analysis. *Journal of Water Resource and Protection, 8*(03), 397.

Hayes, T., Usami, S., Jacobucci, R., & McArdle, J. J. (2015). Using Classification and Regression Trees (CART) and random forests to analyze attrition: Results from two simulations. *Psychology and aging, 30*(4), 911.

Haykin, S., & Arasaratnam, I. (2010). Nonlinear Sequential State Estimation for Solving Pattern-Classification Problems. *Adaptive Signal Processing: Next Generation Solutions, Wiley-IEEE Press, Hoboken, NJ, USA*.

Herrera, G. P., Constantino, M., Tabak, B. M., Pistori, H., Su, J.-J., & Naranpanawa, A. (2019). Long-term forecast of energy commodities price using machine learning. *Energy, 179*, 214-221.

Hosseini, M., & Ashraf, M. A. (2015). *Application of the SWAT model for water components separation in Iran*. Springer.

Isa, D., Lee, L. H., Kallimani, V., & Rajkumar, R. (2008). Text document preprocessing with the Bayes formula for classification using the support vector machine. *IEEE Transactions on Knowledge and Data engineering, 20*(9), 1264-1272.

Jamsran, B.-E., Lin, C., Byambakhuu, I., Raash, J., & Akhmadi, K. (2019). Applying a support vector model to assess land cover changes in the Uvs Lake Basin ecoregion in Mongolia. *Information processing in agriculture, 6*(1), 158-169.

Kiefer, R. W., Lillesand, T. M., & Chipman, J. (1994). *Remote sensing and image interpretation*. Wiley & Sons New York.

Lambin, E. F. (2001). Global land-use and land-cover change: what have we learned so far? *Global Change News, 46*, 27-30.

Lambin, E. F., Geist, H. J., & Lepers, E. (2003). Dynamics of land-use and land-cover change in tropical regions. *Annual review of environment and resources, 28*(1), 205-241.

Lillesand, T., Kiefer, R. W., & Chipman, J. (2015). *Remote sensing and image interpretation*. John Wiley & Sons.

Lin, K.-C., & Hsieh, Y.-H. (2015). Classification of medical datasets using SVMs with hybrid evolutionary algorithms based on endocrine-based particle swarm optimization and artificial bee colony algorithms. *Journal of medical systems, 39*, 1-9.

Lu, D., & Weng, Q. (2007). A survey of image classification methods and techniques for improving classification performance. *International journal of Remote sensing, 28*(5), 823-870.

Luan, H., & Tsai, C.-C. (2021). A review of using machine learning approaches for precision education. *Educational Technology & Society, 24*(1), 250-266.

Mango, L., Melesse, A., McClain, M., Gann, D., & Setegn, S. (2010). Modeling the impact of land use and climate change scenarios of on the hydrology of the upper Mara River, Kenya.

Meyer, W. B., & BL Turner, I. (1994). *Changes in land use and land cover: a global perspective* (Vol. 4). Cambridge University Press.

Mohamoud, Y. M. (1991). Evaluating the Green and Ampt infiltration parameter values for tilled and crusted soils. *Journal of hydrology, 123*(1-2), 25-38.

Mohan, S., & Shrestha, M. N. (2000). A GIS based integrated model for assessment of hydrological changes due to land-use modifications. Symposium on restoration of lakes and wetlands,

Naghibi, S. A., & Dashtpagerdi, M. M. (2017). Evaluation of four supervised learning methods for groundwater spring potential mapping in Khalkhal region (Iran) using GIS-based features. *Hydrogeology journal, 25*(1), 169.

Najafi, M., Moradkhani, H., & Jung, I. (2011). Assessing the uncertainties of hydrologic model selection in climate change impact studies. *Hydrological Processes, 25*(18), 2814-2826.

Navarro, J. A. (2017). First experiences with google earth engine. International Conference on Geographical Information Systems Theory, Applications and Management,

Neetu, & Ray, S. (2019). Exploring machine learning classification algorithms for crop classification using Sentinel 2 data. *The International Archives of the Photogrammetry, Remote Sensing and Spatial Information Sciences, 42*, 573-578.

Neitsch, S. L. (2005). Soil and water assessment tool. *User's Manual Version 2005, 476*.

Neitsch, S. L., Arnold, J. G., Kiniry, J. R., & Williams, J. R. (2011). *Soil and water assessment tool theoretical documentation version 2009*.

Nurfadila, J., Baja, S., Neswati, R., Rukmana, D., & Zylshal, Z. (2019). Initial results on landuse/landcover classification using pixel-based random forest algorithm on Sentinel-2 imagery over Enrekang region. IOP Conference Series: Earth and Environmental Science,

Oki, T., & Kanae, S. (2006). Global hydrological cycles and world water resources. *science, 313*(5790), 1068-1072.

Oliphant, A. J., Thenkabail, P. S., Teluguntla, P., Xiong, J., Gumma, M. K., Congalton, R. G., & Yadav, K. (2019). Mapping cropland extent of Southeast and Northeast Asia using multi-year time-series Landsat 30-m data using a random forest classifier on the Google Earth Engine Cloud. *International Journal of Applied Earth Observation and Geoinformation, 81*, 110-124.

Omar, K. S., Mondal, P., Khan, N. S., Rizvi, M. R. K., & Islam, M. N. (2019). A machine learning approach to predict autism spectrum disorder. 2019 International conference on electrical, computer and communication engineering (ECCE),

Piao, S., Friedlingstein, P., Ciais, P., de Noblet-Ducoudré, N., Labat, D., & Zaehle, S. (2007). Changes in climate and land use have a larger direct impact than rising CO2 on global river runoff trends. *Proceedings of the National Academy of Sciences, 104*(39), 15242-15247.

Potopová, V., Zahradníček, P., Štěpánek, P., Türkott, L., Farda, A., & Soukup, J. (2017). The impacts of key adverse weather events on the field-grown vegetable yield variability in the Czech Republic from 1961 to 2014. *International Journal of Climatology, 37*(3), 1648-1664.

Pretty, J., Sutherland, W. J., Ashby, J., Auburn, J., Baulcombe, D., Bell, M., Bentley, J., Bickersteth, S., Brown, K., & Burke, J. (2010). The top 100 questions of importance to

the future of global agriculture. *International journal of agricultural sustainability, 8*(4), 219-236.

Qian, J., Zhou, Q., & Hou, Q. (2007). Comparison of pixel-based and object-oriented classification methods for extracting built-up areas in arid zone. ISPRS workshop on updating Geo-spatial databases with imagery & the 5th ISPRS workshop on DMGISs,

Razavi, T., & Coulibaly, P. (2013). Streamflow prediction in ungauged basins: review of regionalization methods. *Journal of hydrologic engineering, 18*(8), 958-975.

Rezaee, M., Mahdianpari, M., Zhang, Y., & Salehi, B. (2018). Deep convolutional neural network for complex wetland classification using optical remote sensing imagery. *IEEE Journal of Selected Topics in Applied Earth Observations and Remote Sensing, 11*(9), 3030-3039.

Sahoo, B. B., Jha, R., Singh, A., & Kumar, D. (2019). Application of support vector regression for modeling low flow time series. *KSCE Journal of Civil Engineering, 23*, 923-934.

Sazib, N., Mladenova, I., & Bolten, J. (2018). Leveraging the Google Earth Engine for drought assessment using global soil moisture data. *Remote sensing, 10*(8), 1265.

Semenova, O., & Beven, K. (2015). Barriers to progress in distributed hydrological modelling. *Hydrological Processes, 29*(8), 2074-2078.

Shi, D., & Yang, X. (2015). Support vector machines for land cover mapping from remote sensor imagery. *Monitoring and Modeling of Global Changes: A Geomatics Perspective*, 265-279.

Shiferaw, H., Gebremedhin, A., Gebretsadkan, T., & Zenebe, A. (2018). Modelling hydrological response under climate change scenarios using SWAT model: the case of Ilala watershed, Northern Ethiopia. *Modeling Earth Systems and Environment, 4*, 437-449.

Singh, A. (1989). Review article digital change detection techniques using remotely-sensed data. *International journal of Remote sensing, 10*(6), 989-1003.

Singh, V. P., & Woolhiser, D. A. (2002). Mathematical modeling of watershed hydrology. *Journal of hydrologic engineering, 7*(4), 270-292.

Siroky, D. S. (2009). Navigating random forests and related advances in algorithmic modeling.

Siry, J. P., Cubbage, F. W., & Ahmed, M. R. (2005). Sustainable forest management: global trends and opportunities. *Forest policy and Economics, 7*(4), 551-561.

Sivapalan, M., Takeuchi, K., Franks, S., Gupta, V., Karambiri, H., Lakshmi, V., Liang, X., McDonnell, J., Mendiondo, E., & O'connell, P. (2003). IAHS Decade on Predictions in Ungauged Basins (PUB), 2003–2012: Shaping an exciting future for the hydrological sciences. *Hydrological sciences journal, 48*(6), 857-880.

Srinivasan, R., Ramanarayanan, T. S., Arnold, J. G., & Bednarz, S. T. (1998). Large area hydrologic modeling and assessment part II: model application 1. *JAWRA Journal of the American Water Resources Association, 34*(1), 91-101.

Supe, H., Avtar, R., Singh, D., Gupta, A., Yunus, A. P., Dou, J., A. Ravankar, A., Mohan, G., Chapagain, S. K., & Sharma, V. (2020). Google earth engine for the detection of soiling on photovoltaic solar panels in arid environments. *Remote sensing, 12*(9), 1466.

Taalab, K., Cheng, T., & Zhang, Y. (2018). Mapping landslide susceptibility and types using Random Forest. *Big Earth Data, 2*(2), 159-178.

Tahir, M., Ghattas, M., Birhanu, D., & Nawaz, S. N. (2009). *Cisco IOS XR Fundamentals*. Pearson Education India.

Tahmassebipoor, N., Rahmati, O., Noormohamadi, F., & Lee, S. (2016). Spatial analysis of groundwater potential using weights-of-evidence and evidential belief function models and remote sensing. *Arabian Journal of Geosciences, 9*, 1-18.

Tamiminia, H., Salehi, B., Mahdianpari, M., Quackenbush, L., Adeli, S., & Brisco, B. (2020). Google Earth Engine for geo-big data applications: A meta-analysis and systematic review. *ISPRS journal of photogrammetry and remote sensing, 164*, 152-170.

Tibebe, D., & Bewket, W. (2011). Surface runoff and soil erosion estimation using the SWAT model in the Keleta watershed, Ethiopia. *Land Degradation & Development, 22*(6), 551-564.

Tkassahun, H., Engda, T., Collick, A., Oumer, H. A., Bayabil, H. K., Zewdie, T., Solomon, D., Nicholson, C., & Steenhuis, T. (2009). The Effect of Land Use and Its Management Practices on Plant Nutrient Availability and Carbon Sequestration. *Ethiopia Report*.

Tufa, D. F., Abbulu, Y., & Rao, G. (2015). Hydrological impacts due to land-use and land-cover changes of Ketar watershed, Lake Ziway catchment, Ethiopia. *Int. J. Civ. Eng Tech, 6*, 36-45.

Vandewiele, G., & Elias, A. (1995). Monthly water balance of ungauged catchments obtained by geographical regionalization. *Journal of hydrology, 170*(1-4), 277-291.

Wahap, N., & Shafri, H. Z. (2020). Utilization of Google earth engine (GEE) for land cover monitoring over Klang Valley, Malaysia. IOP Conference Series: Earth and Environmental Science,

Wu, L., Zhao, W., Yang, Z., & Saraf, A. (2023). *Geo-information for Geohazard and Georisk*. Frontiers Media SA.

Xue, C., Chen, B., & Wu, H. (2014). Parameter uncertainty analysis of surface flow and sediment yield in the Huolin Basin, China. *Journal of hydrologic engineering, 19*(6), 1224-1236.

Zaitunah, A., & Manurung, J. (2018). Analysis of Forest Landscape Fragmentation in Samosir Island, North Sumatra. IOP Conference Series: Earth and Environmental Science,

APPENDICES

APPENDICES A: Google Earth Engine land use land cover mapping codes

/////Section ____1   Sentinel_2 Landsat -----RF

  ////////Load sentinel Landsat

 ////Landsat clou mask

```
function cloudMasklandsat(image){
var cloudMaskL457 = function(image) {
var qa = image.select('pixel_qa');
// If the cloud bit (5) is set and the cloud confidence (7) is high
// or the cloud shadow bit is set (3), then it's a bad pixel.
var cloud = qa.bitwiseAnd(1 << 5)
.and(qa.bitwiseAnd(1 << 7))
.or(qa.bitwiseAnd(1 << 3));
// Remove edge pixels that don't occur in all bands
var mask2 = image.mask().reduce(ee.Reducer.min());
return image.updateMask(cloud.not()).updateMask(mask2);
};
var image = ee.ImageCollection("COPERNICUS/S2_SR")
    .filterDate('2022-03-01','2022-04-01')
    .filter(ee.Filter.lt('CLOUDY_PIXEL_PERCENTAGE', 0.1))
    .filterBounds(AOI)
    .median();
var visParamsTrue = {bands:['B4','B3','B2'],min: 0, max: 2500, gamma:1.1};
Map.addLayer(image.clip(AOI),visParamsTrue,'Sentinel_2022')
```

```
Map.centerObject(AOI,11);
      ////creatinig training data
var training =
Agricultureland.merge(Forestland).merge(Grassland).merge(Urbanarea).merge(Shrublan
d).merge(Bereland)
print(training);
var label = 'class'
var bands = ['B2','B3','B4','B8','QA10']
var input = image.select(bands);
      ///overlay the points on the imagery to get training
var trainImage = input.sampleRegions({
collection:training,
scale:30,
});
var trainigData = trainImage.randomColumn();
var trainSet = trainigData.filter(ee.Filter.lessThan('random',0.8))
var testnSet = trainigData.filter(ee.Filter.greaterThanOrEquals('random',0.8));
        //// delet the nul
      // ///Filter out the null property values and try again.
var trainingNoNulls =
trainImage.filter(ee.Filter.notNull( trainImage.first().propertyNames()));
    //// Classification  model
var classifier = ee.Classifier.smileRandomForest(100).train(trainingNoNulls , 'class',
bands);
var classified = image.select(bands).classify(classifier)
Map.addLayer(classified.clip(AOI), {min: 0, max: 5, palette: ['#d63000', '#56cc67',
'#c7e460', '#6cfcff', '#ff60f6','#4b31c2']},'classification 2022RF');
      ///merg into one feature collection
var valNames =
vAgri.merge(vForest).merge(vGrass).merge(vUrban).merge(vShrub).merge(vBarre);
var validation = classified.sampleRegions({
```

```
collection:valNames,
  properties:['class'],
  scale:30,
});
print(validation)
          /////compare the land cover of your validation dataagainst the classification
var testAccuracy = validation.errorMatrix('class','classification');
          /////print error matrix to the console
print('validation error matrix:',testAccuracy);
            ////print the overall accurancy of the console
print('validation overall accuracy:',testAccuracy.accuracy());
print(classifier.confusionMatrix().kappa(), 'kappa');
print(classifier.confusionMatrix(), 'matrix');
```

APPENDICES: Confusion Matrix

Appendices B: CART algorithm confusion Matrix for 2022

	Agriculture	Forest	Grass	Urban	Shrub	Barre	sum	User Accuracy (%)	Commission Error (%)
Agriculture	43	0	11	3	0	3	60	71.67	28.33
Forest	3	51	0	1	1	0	56	91.07	8.93
Grass	10	0	38	1	3	3	55	69.09	30.91
Urban	3	0	0	57	0	0	60	95.00	5.00
Shrub	3	6	2	0	39	0	50	78.00	22.00
Barre	6	0	5	0	0	39	50	78.00	22.00
Sum	68	57	56	62	43	45			
Procedure Accuracy (%)	63.24	89.47	67.86	91.94	90.70	86.67			
Omission Error (%)	36.76	10.53	32.14	8.06	9.30	13.33			

Overall accuracy 80.66%

Kappa value 78.3%.

Appendices C: SVM algorithm confusion Matrix for 2022

	Agriculture	Forest	Grass	Urban	Shrub	Barre	sum	User Accuracy (%)	Commission Error (%)
Agriculture	57	0	3	0	0	0	60	95.00	5.00
Forest	0	55	0	1	0	0	56	98.21	1.79
Grass	35	0	16	1	2	1	55	29.09	70.91
Urban	4	0	1	55	0	0	60	91.67	8.33
Shrub	7	2	0	0	41	0	50	82.00	18.00
Barre	2	0	8	0	0	40	50	80.00	20.00
Sum	105	57	28	57	43	41			
Procedure Accuracy (%)	54.29	96.49	57.14	96.49	95.35	97.56			
Omission Error (%)	45.71	3.51	42.86	3.51	4.65	2.44			

Overall accuracy 79.75%1

Kappa value 57.45%.

Appendices D: NB algorithm confusion Matrix for 2022

	Agriculture	Forest	Grass	Urban	Shrub	Barre	sum	User Accuracy (%)	Commission Error (%)
Agriculture	28	0	6	0	1	25	60	46.67	53.33
Forest	0	51	0	1	4	0	56	91.07	8.93
Grass	16	0	22	1	13	3	55	40.00	60.00
Urban	2	0	0	54	0	4	60	90.00	10.00
Shrub	0	16	0	0	34	0	50	68.00	32.00
Barre	0	0	1	0	0	49	50	98.00	2.00
Sum	46	67	29	56	52	81			
Procedure Accuracy (%)	60.87	76.12	75.86	96.43	65.38	60.49			
Omission Error (%)	39.13	23.88	24.14	3.57	34.62	39.51			

Overall accuracy 71.90%

Kappa value 38.32%.

Appendices E: RF algorithm confusion matrix for the year 1997 LULC map

	Agriculture	Forest	Grass	Urban	Shrub	Barre	sum	User Accuracy (%)	Commission Error (%)
Agriculture	41	0	3	0	0	1	45	91.11%	8.89%
Forest	1	42	1	0	1	0	45	93.33%	6.67%
Grass	2	0	37	0	2	0	41	90.24%	9.76%
Urban	2	1	0	44	3	0	50	88.00%	12.00%
Shrub	1	1	2	0	34	0	38	89.47%	10.53%
Barre	2	0	0	0	1	40	43	93.02%	6.98%
Sum	49	44	43	44	41	41			
Procedure Accuracy %	83.67	95.45	86.05	100	82.93	97.56			
Omission Error %	16.33	4.55	13.95	0.00	17.07	2.44			

Overall accuracy 90.83%

Kappa 98.71%

Appendices F: RF algorithm confusion matrix for the year 2010 LULC map

	Agriculture	Forest	Grass	Urban	Shrub	Barre	sum	User Accuracy	Commission Error
Agriculture	43	0	1	2	2	0	48	89.58%	10.42%
Forest	0	31	1	1	10	1	44	70.45%	29.55%
Grass	2	0	37	2	1	3	45	82.22%	17.78%
Urban	1	0	1	41	1	3	47	87.23%	12.77%
Shrub	0	2	1	0	39	1	43	90.70%	9.30%
Barre	2	0	2	1	0	39	44	88.64%	11.36%
Sum	48	33	43	47	53	47			
Procedure Accuracy %	89.58	93.94	86.05	87.23	73.58	82.98			
Omission Error%	10.42	6.06	13.95	12.77	26.42	17.02			

Overall accuracy 84.87%

Kappa 98.58%

Sensitivity analysis parameters

Appendices G: Parameters used in Sensitivity analysis

Parameter Name	t-Stat	P-Value
11:R__SLSUBBSN.hru	0.02	0.99
7:V__BIOMIX.mgt	0.11	0.91
14:R__CH_N2.rte	0.12	0.91
20:R__REVAPMN.gw	0.37	0.71
19:R__SURLAG.bsn	-0.49	0.63
9:A__SOL_AWC(..).sol	0.60	0.55
18:R__ESCO.bsn	-0.64	0.52
16:R__ALPHA_BNK.rte	0.65	0.51
8:A__CH_K2.rte	-0.76	0.45
13:R__GWQMN.gw	0.88	0.38
12:R__RCHRG_DP.gw	0.89	0.37
4:V__OV_N.hru	-1.35	0.18
21:R__TLAPS.sub	-1.37	0.17
10:R__GW_DELAY.gw	-1.40	0.16
3:V__HRU_SLP.hru	1.62	0.11
15:R__SOL_ALB(..).sol	1.79	0.07
6:A__EPCO. hru	2.13	0.03
5:V__ALPHA_BF.gw	-2.36	0.02
1:A__SOL_K(..).sol	-2.70	0.01
17:R__CANMX.hru	2.82	0.00
2:V__CN2.mgt	-13.96	0.00

Appendices H: Top 10 Sensitive parameters for 2010

4:V__OV_N.hru	-1.35	0.18
21:R__TLAPS.sub	-1.37	0.17
10:R__GW_DELAY.gw	-1.40	0.16
3:V__HRU_SLP.hru	1.62	0.11
15:R__SOL_ALB(..).sol	1.79	0.07
6:A__EPCO.bsn	2.13	0.03
5:V__ALPHA_BF.gw	-2.36	0.02
1:A__SOL_K(..).sol	-2.70	0.01
17:R__CANMX.hru	2.82	0.00
2:V__CN2.mgt	-13.96	0.00

Appendices I: Top 10 sensitive parameters for 2022

9:A__SOL_AWC (..).sol	1.27	0.20
10:R__GW_DELAY.gw	-1.62	0.11
20:R__REVAPMN.gw	-1.75	0.08
3:V__HRU_SLP.hru	1.81	0.07
17:R__CANMX.hru	2.18	0.03
16:R__ALPHA_BNK.rte	2.39	0.02
1:A__SOL_K(..).sol	-2.54	0.01
5:V__ALPHA_BF.gw	-10.06	0.00
13:R__GWQMN.gw	12.68	0.00
2:V__CN2.mgt	16.40	0.00

APPENDICES J: - 95PPU plot
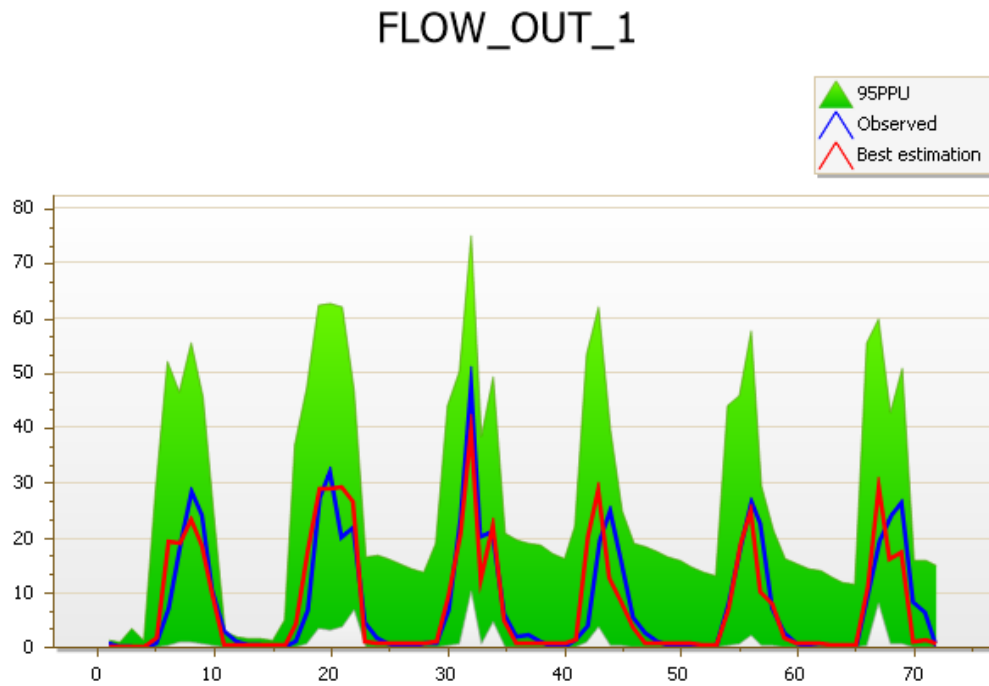
Appendices D: 95PPU for Best Simulation